Part III

X-Ray and Optical Observations of SSS

Supersoft X-Ray Sources in M 31

J. Greiner[1], R. Supper[1], E.A. Magnier[2,3]

[1] Max-Planck-Institute for Extraterrestrial Physics, 85740 Garching, Germany
[2] University of Amsterdam, Astronomy Dept, 1098 SJ Amsterdam, The Netherlands
[3] University of Washington, Dept of Astronomy FM-20, Seattle, WA 98195, USA

1 Introduction

As the most massive galaxy in the Local Group the early-type spiral M31 is close enough to be studied in detail at various wavelengths. A ROSAT PSPC mosaic of 6 contiguous pointings with an exposure time of 25 ksec each was performed in July 1991 (first M31 survey). A raster pointing of 80 observations with 2.5 ksec exposure time each covering the whole M31 disk was made in July/August 1992 and January 1993 (second M31 survey). A multi-step detection algorithm involving a maximum likelihood technique as final step was applied to the individual pointings of the first survey with a likelihood threshold of 10. A total of 396 X-ray sources were detected within the field of view of about 6.3 deg^2 (Supper et al. 1996). For each source several quantites are determined such as the position, the total number of background subtracted counts, the corresponding countrate and two hardness ratios for a crude spectral characterisation.

CCD photometry has been performed in four passbands (*BVRI*) of the entire optical disk of M31 in September 1990 and September 1991 using the McGraw-Hill 1.3m telescope of the Michigan-Dartmouth-MIT Observatory at Kitt Peak (Magnier et al. 1992, Haiman et al. 1993). The observations have typical completeness limits of (22.3,22.2,22.2,20.9). Different selection criteria on these data sets allow the extraction of different classes of objects. Of particular interest are likely Galactic foreground stars which have been identified with the criteria V$\leq$18 and B–V>0.4 (predominantly main sequence and giant stars).

2 Selection Criteria and Source Sample

Two selection criteria were applied to the total sample of detected X-ray sources:

- the hardness ratio has to satisfy HR1 + $\sigma_{\rm HR1} \leq -0.80$. The hardness ratio HR1 is defined as the normalized count difference (N_{50-200} – N_{10-40})/(N_{10-40} + N_{50-200}), where N_{a-b} denotes the number of counts in the PSPC between channels a and b. Similarly, HR2 is defined as (N_{91-200} – N_{50-90})/N_{50-200}. We note that HR1 is sensitive to the absorbing column, and that HR2 is basically zero (within the errors) for supersoft sources. The error in the hardness ratio ($\sigma_{\rm HR1/2}$) was calculated by applying Gaussian error propagation.
- no correlation with any optical object in the error box which has been classified as a foreground object.

Table 1. Summary of the supersoft X-ray sources in M31 according to our selection criteria (see text for details) plus the source proposed by White et al. (1995) as supersoft transient (last row). Given for each source are the name (column 1), the best fit X-ray position (2), the 3σ location error (3), the total number of counts collected in the corresponding pointing (exception: for the White et al. source all pointings are used; 4), the PSPC countrate in the 0.1-2.4 keV band (5), the hardness ratio HR1 with error (6), the hardness ratio HR2 with error (7), and the maximum blackbody temperature (8, see text).

Name	Coordinate (2000.0)	Error ($''$)	N_{cts}	countrate (cts/ksec)	HR1	HR2	T_{bb}^{max} (eV)
RX J0037.4+4015	$00^h37^m25\overset{s}{.}3$ $+40°15'16''$	18	10	0.31±0.31	−0.93±0.07	0.02±0.71	43
RX J0038.5+4014	$00^h38^m32\overset{s}{.}1$ $+40°14'39''$	33	33	0.80±0.28	−0.92±0.08	−0.49±0.53	45
RX J0038.6+4020	$00^h38^m40\overset{s}{.}9$ $+40°20'00''$	15	74	1.73±0.29	−0.93±0.06	0.32±0.66	43
RX J0039.6+4054	$00^h39^m38\overset{s}{.}5$ $+40°54'09''$	21	22	0.44±0.44	−0.92±0.07	−0.04±0.71	45
RX J0040.4+4009	$00^h40^m26\overset{s}{.}3$ $+40°09'01''$	27	31	0.85±0.32	−0.94±0.06	−0.90±0.10	42
RX J0040.7+4015	$00^h40^m43\overset{s}{.}2$ $+40°15'18''$	21	50	1.26±0.32	−0.94±0.06	−0.31±0.64	42
RX J0041.5+4040	$00^h41^m30\overset{s}{.}2$ $+40°40'04''$	18	16	0.32±0.18	−0.95±0.05	−0.62±0.44	40
RX J0041.8+4059	$00^h41^m49\overset{s}{.}9$ $+40°59'21''$	27	23	0.49±0.24	−0.93±0.07	−0.63±0.43	43
RX J0042.4+4044	$00^h42^m27\overset{s}{.}6$ $+40°44'32''$	15	72	1.69±0.32	−0.93±0.07	−0.07±0.70	43
RX J0043.5+4207	$00^h43^m35\overset{s}{.}9$ $+42°07'30''$	15	57	2.15±0.55	−0.92±0.08	−0.27±0.66	45
RX J0044.0+4118	$00^h44^m04\overset{s}{.}8$ $+41°18'20''$	15	69	2.46±0.42	−0.94±0.06	0.11±0.81	42
RX J0045.5+4206	$00^h45^m32\overset{s}{.}3$ $+42°06'59''$	24	86	3.14±0.34	−0.89±0.07	−0.29±0.65	42
RX J0046.2+4144	$00^h46^m15\overset{s}{.}6$ $+41°44'36''$	15	63	2.15±0.39	−0.93±0.07	0.62±0.40	38
RX J0046.2+4138	$00^h46^m17\overset{s}{.}8$ $+41°38'48''$	27	30	1.12±0.40	−0.91±0.09	−0.27±0.65	40
RX J0047.6+4205	$00^h47^m38\overset{s}{.}5$ $+42°05'07''$	30	29	1.05±0.36	−0.92±0.07	0.06±0.70	39
RX J0045.4+4154	$00^h45^m29\overset{s}{.}0$ $+41°54'08''$	18	1040	29.63±0.98	+0.78±0.03	−0.59±0.03	128

Among all 396 detected sources a total of 15 fulfill these two requirements. These sources are listed in Tab. 1 and are identical to the sources #3, #12, #18, #39, #78, #88, #114, #128, #171, #245, #268, #309, #335, #341, and #376 in Supper et al. (1996). Fig. 1 shows the positions of these sources overplotted on an optical image of M31.

3 X-Ray Characteristics

We have applied a spectral fit only to the brightest source of our sample, namely RX J0045.5+4206. A blackbody model fit gives an absorbing column of 1.2×10^{21} cm^{-2}, a factor of two higher than the Galactic value (0.6×10^{21} cm^{-2}, Dickey and Lockman 1990). But the uncertainty is large, and the line of sight Galactic absorption is well within the 3σ contour (see Fig. 2). The resulting blackbody temperature is 30^{+20}_{-10} eV at the Galactic absorbing column, similar to the known supersoft sources (Greiner et al. 1991, Kahabka et al. 1994). The bolometric luminosity for this model blackbody is about 7×10^{37} erg/s. A comparison of blackbody and white dwarf atmosphere models has shown that while the temperature estimates did not differ much, the bolometric luminosity can be a factor 10–100 lower when using a white dwarf atmosphere model (Heise et al. 1994). We there-

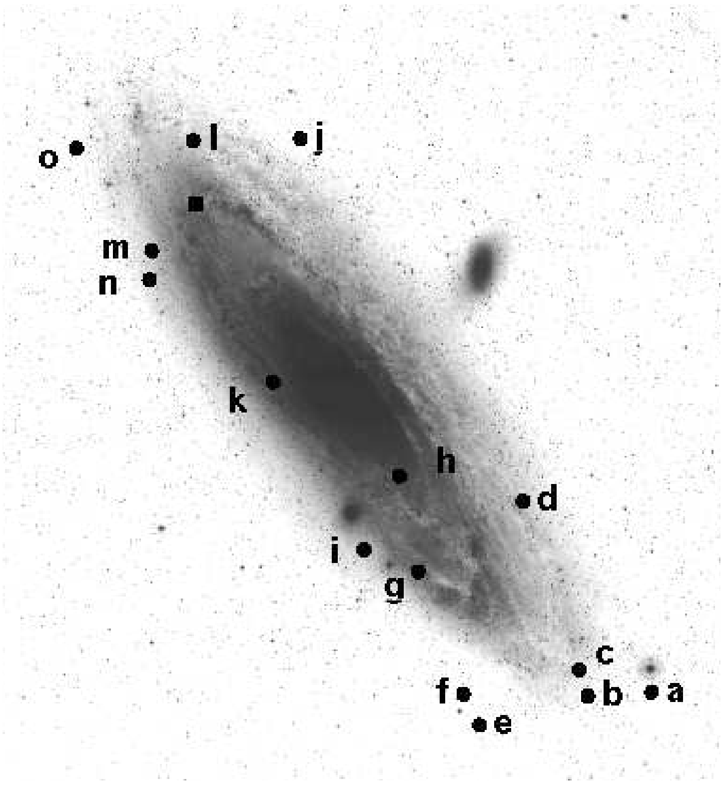

Fig. 1. The location of the 15 supersoft sources plotted over an optical image (POSS O plate) of M31. Letters (a through o) denote the X-ray sources in Tab. 1 from top to bottom. The source RX J0045.4+4154 (White et al. 1995) is shown as a square. Sources h, k and l have objects brighter than 20th mag in their X-ray error box (see text for possible counterpart types). Sources e and m lie at the edge of the *BVRI* survey field, while a, j and n are outside of this survey.

fore think that the above given bolometric luminosity derived at the Galactic absorbing column should be a better representation than the best-fit value.

In order to get some crude spectral information also for the other, fainter X-ray sources we have adopted the following scheme: We calculate the hardness ratio HR1 for blackbody models with different temperatures and absorbing columns (Fig. 3). We then take the measured HR1 value, and determine the model blackbody temperature at the Galactic absorbing column. Since for a given hardness ratio the temperature decreases with increasing N_H, these temperatures are upper limits. As could be expected already from the rather similar values of HR1, these maximum blackbody temperatures lie in a quite narrow range between 40–50 eV (last column in Tab. 1).

Recently, White et al. (1995) have reported on a recurrent X-ray transient which they claim to be supersoft. We have determined the maximum temper-

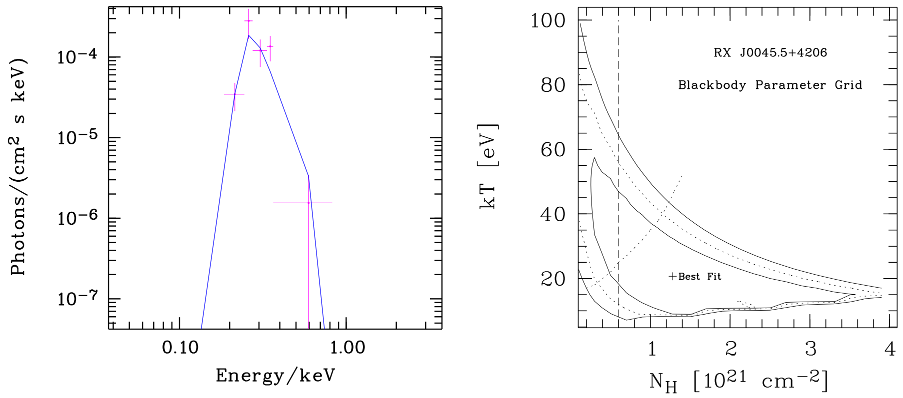

Fig. 2. Best fit blackbody model of the brightest of our supersoft X-ray sources RX J0045.5+4206 (left) and the $1, 2, 3\sigma$ error contours in the $kT - N_H$ plane (right panel). Only photons from one single 25 ksec pointing are used. Some photons had to be discarded because of another bright source at only 1!8 distance making the flux somewhat uncertain. Due to small photon numbers, the parameter range is not too well constrained. and thus introduces an additional uncertainty in the luminosity. In the right panel the dashed vertical line corresponds to the mean total Galactic absorption, and the dotted line marks the Eddington limit of the blackbody model.

ature with the same method as our source sample, using the merged pointings of the second PSPC survey of M31. This temperature and the hardness ratio of this source (Tab. 1) clearly demonstrate that it is considerably harder than the sources we have extracted here. From the spectral similarity we speculate that it is rather a Her X-1 like object than a supersoft X-ray source.

All 15 X-ray sources have been checked for temporal variability against the August 1992 observations of the second M31 survey. None of the sources fulfilled the criterion for variability (flux difference in the two observations divided by the quadratic sum of the flux errors has to be larger than 3σ).

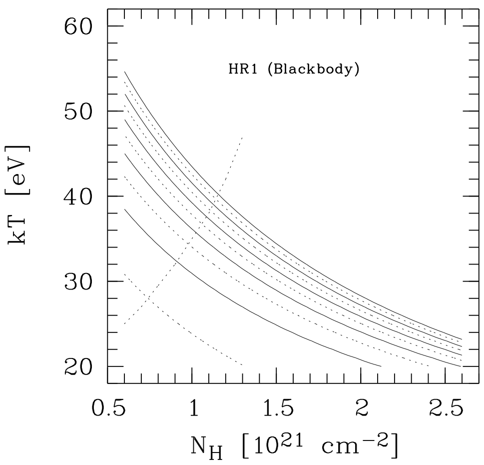

Fig. 3. The hardness ratio HR1 as a function of blackbody temperature kT and absorption column density N_H. HR1 increases from the upper line with HR1= -0.80 to the bottom line with HR1= -0.98 in steps of 0.02. For a given hardness ratio the blackbody temperature decreases with increasing column density. Therefore, the kT value at $N_H = 0.6 \times 10^{21}$ cm^{-2} gives the maximum blackbody temperature. The dotted line marks the Eddington limit of the blackbody model.

4 Source Positions and Identifications

The 396 X-ray source positions as they result from the maximum likelihood detection algorithm have varying errors depending on the off-axis angle in the field of view of the PSPC. Since for nearly a quarter of X-ray sources optical counterparts could be identified due to the positional coincidence plus the colour information from the *BVRI* survey, we have used a subset of these optically identified X-ray sources (namely the 29 globular clusters) to improve the systematic errors in the X-ray source determination. We have determined the matrix coefficients for a unique rotation plus translation which gives the smallest residual position differences for the optical and X-ray positions of the optically identified X-ray sources. The same matrix has then been applied to all X-ray sources.

There are several source positions (Fig. 1) with optical objects inside the error box. The optical selection criterion is effective mainly against red objects of some of our supersoft sources. Single, i.e. non-interacting white dwarfs (WDs) and many magnetic cataclysmic variables (CVs) also have supersoft X-ray spectra, and such objects are blue. From the known ratio of optical to X-ray luminosity and the observed X-ray fluxes we might expect Galactic, single WDs at typical V magnitudes of 18–20 mag and CVs at even fainter magnitudes. These type of objects thus constitute a possible contamination of our sample. In particular, objects RX J0041.8+4059, RX J0044.0+4118 and RX J0045.5+4206 have blue objects of 19–20th mag in their respective error box, and thus might be Galactic WDs or CVs. On the other hand, blue stars in M31 are not distributed randomly, but in the spiral arms. The above mentioned objects are in regions with many blue stars, i.e. in associations. Thus, the probability of having a coincident CV or WD in these areas is not the sky density of CVs or WDs times the area of the survey, but rather only times the total area of the associations, which is substantially smaller. Spectroscopic observations are clearly necessary to distinguish between these alternatives.

There is recent evidence that also some active galactic nuclei (AGN) have supersoft X-ray spectra (Greiner et al. 1996). At least one AGN (WPVS007, Grupe et al. 1995) has HR1<–0.8, and there are a number of further secure identifications with HR1<–0.6. We therefore caution that one or the other source in our list which is located in the outskirts of M31 might be an AGN shining through M31. RX J0040.4+4009 and RX J0040.7+4015 are plausible candidates.

In addition to the *BVRI* survey, images were also aquired in the Hα line. Only five of the sources turned out to lie in the Hα fields: RX J0040.7+4015, RX J0041.5+4040, RX J0041.8+4059, RX J0042.4+4044 and RX J0044.0+4118. None of these reveals any Hα emission. The upper limits in Hα luminosity are 10^{35} erg/s, i.e. a CAL 83 like nebula (Pakull & Motch 1989, Remillard et al. 1995) would have been detected. This result is not surprising in view of the fact that in a search for nebulae around known supersoft sources in the Galaxy and the Magellanic Clouds only one out of 10 sources has revealed a nebula (Remillard et al. 1995).

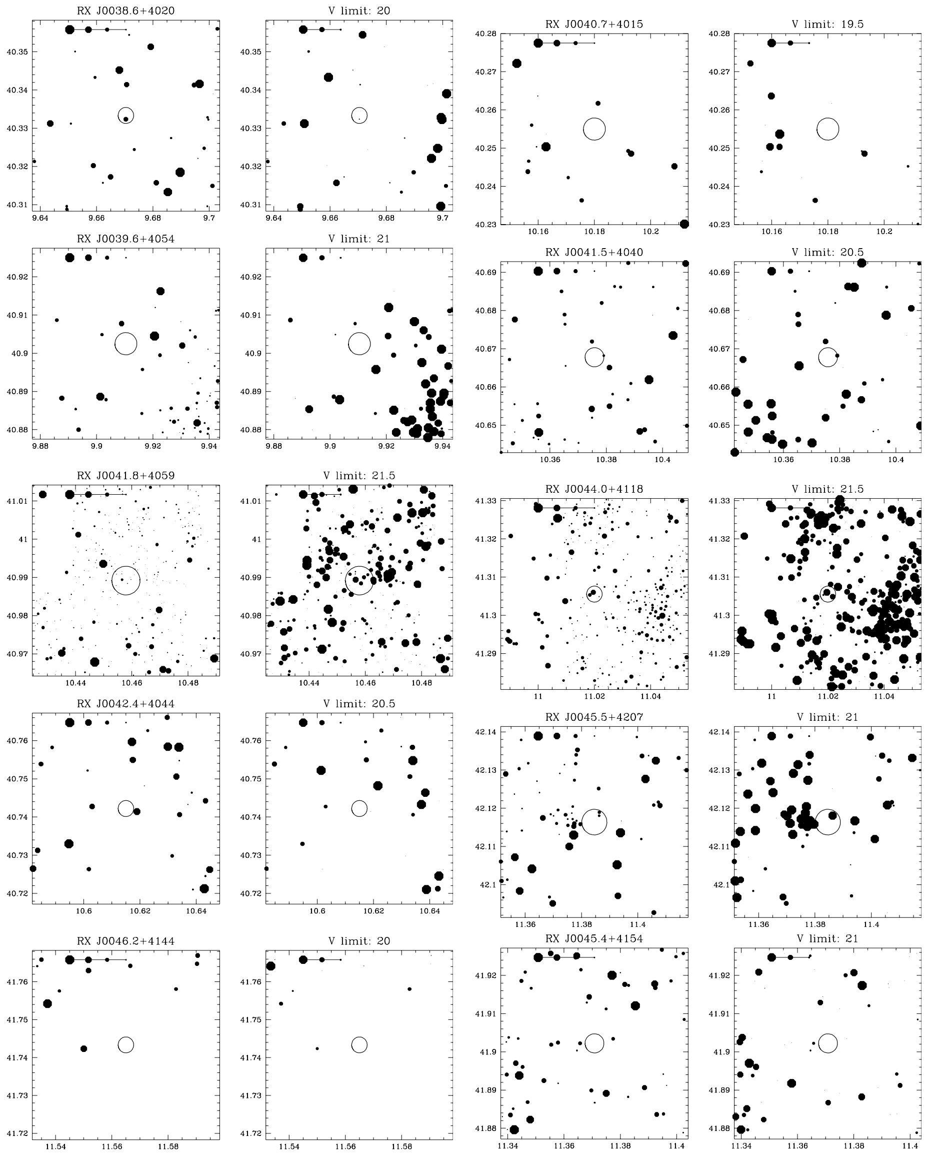

Fig. 4. Finding charts for those supersoft sources covered by the *BVRI* survey which have V limiting magnitudes fainter than 20 mag. For each source two panels are given: The right (with the ROSAT name on the top) is the V image with the dot size scaled according to the brightness with the scaling of V=15,17,19,21 shown in the upper left. In the right panel (with the limiting V magnitude on top) the size is scaled by the color (B-V=0.0,0.4,0.8 from left to right in the upper left scaling).

5 Conclusions

Our selection criterion according to the X-ray hardness ratio is very restrictive. An identical selection criterion has been applied to all sources in the *ROSAT* all-sky survey, and only about 30% of the known supersoft sources in the LMC and SMC were found (Greiner 1996). For instance, even a M31 source identical to CAL 83 would probably been missed with the present selection criterion. This is due to the fact that at lower intensities the error in the hardness ratio increases readily above 0.1–0.15 and removes the sources from the sample. Also, the selection criterion is more sensitive to low-temperature objects, i.e. sources with emission above 0.4 keV are already excluded. Therefore, a more relaxed hardness ratio selection will certainly increase the number of further sources which could qualify as supersoft sources.

The optically brightest supersoft X-ray source in the Large Magellanic Cloud has V=16.2 mag. A similar source in M31 is expected to have V=21.7 mag, still within the range of the *BVRI* survey. Those objects which have optical counterparts brighter than this might be expected not to be burning WDs in close binaries, but possibly Galactic single WDs or CVs or bright blue objects in M31. Also, a supersoft AGN is not excluded a priori as counterpart for X-ray sources in the outskirts of M31. We therefore conclude that not all of the sources described here in more detail may qualify as luminous close binaries like CAL 83 after spectroscopic identification has been succeeded.

The location distribution of our supersoft source sample across M31, especially the lack of sources in the inner bulge, clearly suggests that they belong to the disk population. Therefore, the detection probability is seriously affected by the absorbing column between the source and the observer.

Acknowledgement: JG is supported by the Deutsche Agentur für Raumfahrtangelegenheiten (DARA) GmbH under contract FKZ 50 OR 9201. The *ROSAT* project is supported by the German Bundesministerium für Bildung, Forschung, Wissenschaft und Technologie (BMBW/DARA) and the Max-Planck-Society.

References

Dickey J.M., Lockman F.J., 1990, Ann. Rev. Astron. Astrophys. 28, 215

Greiner J., Hasinger G., Kahabka P. 1991, A&A 246, L17

Greiner J., 1996, this volume p. 285

Greiner J., Danner R., Bade N., Richter G.A., Kroll P., Komossa S., 1996, A&A (in press, MPE prepr. 342)

Grupe D., Beuermann K., Mannheim K., Thomas H.-C., Fink H.H., de Martino D., 1995, A&A 300, L21

Haiman Z., Magnier E.A., Lewin W.H.G., Lester R.R., van Paradijs J., Hasinger G., Pietsch W., Supper R., Trümper J., 1993, A&A 286, 725

Heise J., van Teeseling A., Kahabka P., 1994, A&A 288, L45

Kahabka P., Pietsch W., Hasinger G., 1994, A&A 288, 538

Magnier E.A., Lewin W.H.G., van Paradijs J., Hasinger G., Jain A., Pietsch W., Trümper J., 1992, A&A Supp 96, 379
Magnier E.A., Prins S., van Paradijs J., Lewin W.H.G., Supper R., Hasinger G., Pietsch W., Trümper J., 1995, A&AS 114, 215
Pakull M.W., Motch C., 1989, in Extranuclear Activity in Galaxies, ed. E.J.A. Meurs, R.A.E. Fosbury, (Garching, ESO), p. 285
Remillard R.A., Rappaport S., Macri L.M., 1995, ApJ 439, 646
Supper R., Hasinger G., Pietsch W., Trümper J., Jain A., Magnier E.A., Lewin W.H.G., van Paradijs J., 1996, A&A (in press)
White N.E., Giommi P., Heise J., Angelini L., Fantasia S., 1995, ApJ 445, L125

X-Ray and Optical Observations of RX J0925.7–4758: Constraints on the Binary Structure

C. Motch

CNRS, Observatoire de Strasbourg, 11 rue de l'Université, F-67000 Strasbourg

Abstract. We report on preliminary results from an X-ray and optical observing campaign of the galactic supersoft X-ray source RX J0925.7–4758. The combined analysis of all available V band photometry indicates an orbital period of 3.79 $\pm$ 0.24 d. Medium resolution spectra collected during 5 consecutive nights show that the radial velocities of Hα and He II λ4686 vary together with the $\approx$ 3.8 day cycle and probably exclude short 1 day alias periods. This rather long period and the absence of marked stellar signatures in the optical spectrum indicate that the mass donor is probably a giant or subgiant K4 to A0 type star. A long ROSAT HRI observation reveals that the source is variable from 0.35 to 0.5 cts s^{-1} on a time scale of a few days suggesting that the X-ray flux of RX J0925.7–4758 could be modulated with orbital motion. The phasing of the photometric V band and radial velocity curves is consistent with a model in which the photometric modulation is caused by the heated hemisphere of the companion star and emission lines arise from a region dynamically linked to the X-ray source. If this interpretation is correct, then the companion star may indeed be significantly more massive than the X-ray source as expected in current models of steady nuclear burning supersoft sources.

1 Introduction

So far, only a handful of supersoft sources are known in the Galaxy and most of them have soft X-ray luminosities significantly smaller than those found in the Magellanic Clouds for instance. In particular, soft X-ray galactic surveys, including the ROSAT all-sky survey, failed to detect galactic equivalents of sources like Cal 83 which would yield PSPC count rates as high as 1,000 cts/s if they were located at typical galactic distances. A natural explanation for this is that interstellar absorption in the Galaxy heavily attenuates the soft X-ray emission from these sources and that consequently, their observed X-ray spectra should look quite different from those of their Magellanic counterparts. Using this simple idea led to the discovery of RX J0925.7–4758 in the low galactic latitude part of the ROSAT all-sky survey (Motch Hasinger & Pietsch 1994, hereafter MHP94).

The X-ray spectrum of RX J0925.7-4758 is highly unusual for supersoft sources as it displays peaked emission close to 1 keV with very little flux detected below 0.4 keV and above 1.5 keV. This peculiar energy distribution may be explained by intrinsically soft emission cut off at low energies by photoelectric absorption from a large column density $N_H \approx 10^{22}$ cm^{-2}. Recent ASCA SIS observations by

Ebisawa et al. (1996) reveal the probable presence of several absorption edges such as O VIII (0.9 keV) and Ne X (1.38 keV). The fact that only the very high energy tail of the emitted spectrum can be analyzed and the absence of strong constraints on the distance to the source allow a large range of possible bolometric luminosities (L_{Bol} = $10^{34.8}$ to $\geq 10^{37.7}$ erg s^{-1}, Ebisawa et al. 1996).

RX J0925.7–4758 is identified with a V $\approx$ 17 highly reddened object (E(B-V) = 2.1) suggesting that most, if not all, of the large photoelectric absorption seen in X-rays is of interstellar origin. The optical spectrum is characterized by H_α and high excitation emission lines such as He II λ4686 and the N III - C III Bowen complex. V band photometry shows the presence of a modulation with a probable period in the range of 3.3 - 4.0 d (MHP94).

In this paper, we report on preliminary results from more recent optical photometric and spectroscopic observations and from a 4.1 day long ROSAT HRI observation.

2 Optical Observations

Observations collected in April and December 1992 were already described in MHP94. In February 1994, we obtained five consecutive nights of observations with the ESO 1.52 m telescope and the Boller & Chivens spectrograph. With grating # 23 (129 Å/mm) and CCD #24 FA2K (1.93 Å pixel^{-1}), the FWHM resolution was $\approx$ 4 Å covering the wavelength range between 4000 and 7300 Å. The typical exposure time was 30 min. On occasions, the entrance slit was wide opened to 8.3$''$ and aligned on RX J0925.7–4758 and comparison star 2 in MHP94. From these observations, it was possible to reconstruct a photometric V light curve simultaneous with spectroscopy.

Quasi-simultaneously with the ROSAT observations in June 1994, Dr. S. Mottola kindly obtained V band photometry using the ESO-Dutch 0.9 m telescope at ESO, La Silla and the TEK #29 CCD chip.

2.1 Timing Analysis of the 1992-1994 Photometric V Data

A modulation on a time scale of several days is present during all of the four observing runs. Merging the 1994 February and June photometry with the previously reported 1992 data basically yields the same periodicities as found in MHP94. On the long period side, there is a series of alias peaks in the range P = 3.55 - 4.03 d. Among this set of alias periods, the least square power spectrum (Lomb 1976, Scargle 1982) and the minimum string length periodogram (Dworetsky 1983) both give a 'best' period at P = 3.7790 $\pm$ 0.0020 d with maximum light at JD 2,448,700.88 $\pm$ 0.11 d. This 'best' period is slightly longer, but still consistent with that found in MHP94 (P = 3.55 d). However, since intrinsic variability is likely to be present in the light curve, an accurate determination

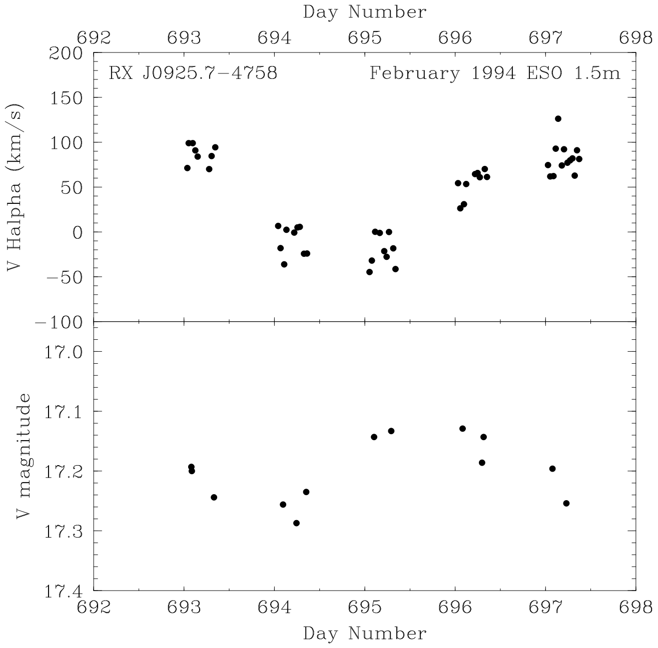

Fig. 1. Simultaneous H_α radial velocity and V magnitude light curves observed in February 1994. Day number is JD - 2,448,700.5.

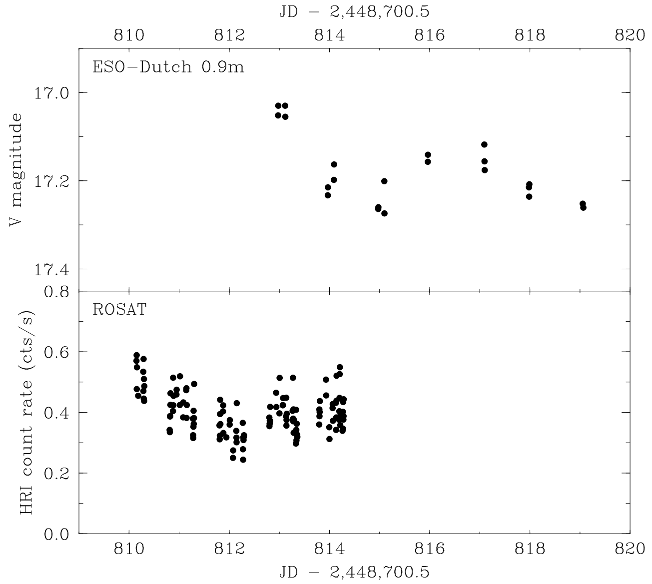

Fig. 2. ROSAT HRI and V photometric light curves obtained in June 1994. X-ray data are averaged into 300 s bins

of the photometric period would require more extended monitoring. For the moment we prefer to retain P = 3.79 ± 0.24 d as a conservative value. An one day alias series of slightly smaller significance occurs at P = 1.37 ± 0.03 d.

2.2 The Radial Velocity Curve

In Fig. 1 we show the H_α radial velocity curve together with the reconstructed V magnitudes. A smooth modulation appears both in the radial velocities and in the photometric light curves. The time scale of variability is compatible with the P = 3.55 - 4.03 d range of photometric periods. From the lack of significant radial velocity changes within a single night (≈ 0.35 days) we conclude that short 1 day alias periods (P $\approx$ 1.37 d and P $\approx$ 0.774 d) are probably excluded.

H_α and He II λ4686 radial velocities vary together in phase. Assuming P = 3.779 d gives $K_{H_\alpha} = 63 \pm 4\,\mathrm{km\,s^{-1}}$ and $K_{HeII} = 84 \pm 30\ \mathrm{km\,s^{-1}}$. The optical photometric maximum occurs at inferior conjunction of the line emitting region, whatever is the exact value of the orbital period.

3 ROSAT HRI Monitoring

In June 1994 ROSAT monitored the source during 4.1 days with an effective exposure time of 55 ksec. We show in Fig. 2 the ROSAT HRI data together with the V band photometry obtained by Dr. S. Mottola with the ESO-Dutch 0.9 m telescope. The scatter in the HRI data is mostly due to photon counting statistics. The only significant variability is the $\approx$ 40% change in the X-ray flux from 0.35 to 0.5 cts/s on a time scale of a few days. Although the duration of the observation is not long enough to exclude the possibility that we simply witnessed a slow random variation, the time scale of variation is nevertheless comparable with the photometric period. Similar orbital phase dependent X-ray modulations are seen in some other supersoft sources (Kahabka 1996), and we may have detected such an effect in RX J0925.7–4758 as well. The maximum of the optical light curve, close to day 813, occurs $\approx$ 0.1-0.2 cycles after X-ray minimum.

4 Discussion

One of the straightforward result of this study is the apparent absence of large long term variations of the mean optical and X-ray flux of the source. From 1992 April till 1994 June the season averaged V magnitude of the optical counterpart did not change by more than a few percents. The source was always detected by ROSAT or ASCA and no X-ray flux variations larger than $\approx$ 50% are present from the survey discovery in 1991 till the most recent 1994 June observations. In the framework of the accreting white dwarf model (van den Heuvel et al. 1992), this behaviour is compatible with a genuine steady nuclear burning source or with a source decaying or rising on a time scale ≥ 3 yr.

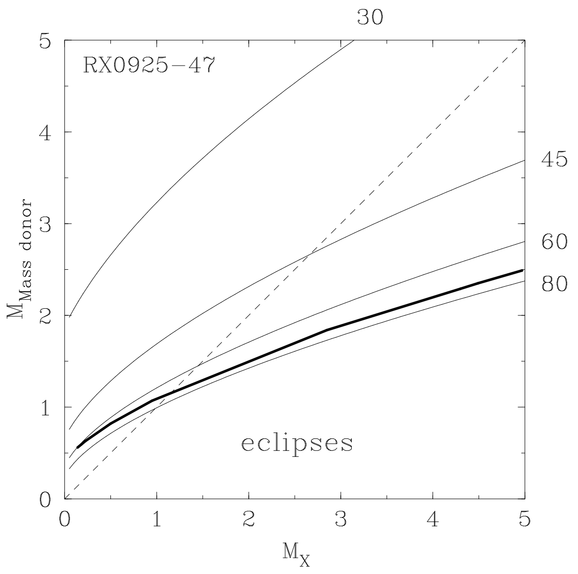

Fig. 3. Mass of the X-ray source plotted against the mass of the companion star for various orbital inclinations. We assume here $K_X = K_{HeII} = 84$ km s^{-1}. The dashed line represent equal masses. Solution below the thick line would produce X-ray eclipses.

The orbital period of RX J0925.7–4758 is most probably long, P = 3.79 ± 0.24 d, so far the longest known for supersoft sources, if one ignores the symbiotic systems. This readily indicates that the mass donor star is evolved. Roche lobe geometry implies a mean density of $\rho \approx 5\,10^{-3}$ - 10^{-2} $\rho_\odot$ for the companion star corresponding to a giant or subgiant configuration. The absence of marked stellar features in the optical spectrum (MHP94) implies that as in other supersoft sources, the optical emission is dominated by the accretion disk, by the wind, and/or by the X-ray heated hemisphere of the companion star. If the visual absolute magnitude of RX J0925.7–4758 is similar to those of the Magellanic Cloud sources (i.e. up to $M_V = -2.1$ for RX J0513.9-6951, Pakull et al. 1993) the mass donor star can not be brighter than $M_V \approx 0.0$, indicating an A0 to K4 giant or subgiant spectral type.

The phasing of the He II λ4686 and H_α emission lines with respect to the optical photometric light curve is such that maximum light occurs when the line emitting region is closest to the observer. A similar behaviour is observed in Her X-1 and Sco X-1 and is generally interpreted by a model in which the high excitation lines are produced close to the X-ray source, probably in the inner region of the accretion disc, while the optical photometric modulation is essentially caused by the varying aspect of the X-ray heated hemisphere of the Roche lobe filling star. A similar phasing is found in the supersoft X-ray source Cal 87 (Cowley et al. 1990) and RX J0019.8+2156 (Beuermann et al. 1995). It has been argued, however, that He II $\lambda 4686$ lines may not exactly reflect the motion of the X-ray source since a sizeable fraction of the line emission may be produced in a wind emanating from the disc or from the companion star. Accordingly, the resulting emission line velocity may be smaller than that of the X-ray source and may even vary in antiphase if the companion star dominates (van den Heuvel et al. 1992). One should note, in addition, that the shape of the photometric light curve of RX J0925.7–4758 may not be compatible with that expected from a single hot stellar hemisphere. The presently available photometric data are still too scarce to allow to distinguish a truly periodic fine structure such as a narrow eclipse or dip from random cycle to cycle variations. However, at the 'best' period of P = 3.779 d, minimizing the scatter in phase, the folded light curve displays a rather peaked maximum with some evidence for a complex narrow absorption feature occuring ≈ 0.1 cycles before photometric maximum and apparently in phase with the X-ray minimum. A bulge on the edge of the accretion disc or a tilted disc such as proposed in Her X-1 (Gerend & Boynton 1976) could possibly explain the detailed features of the photometric light curve. The surprising occurrence of the X-ray minimum close to inferior conjunction of the X-ray source may reflect the fact that because of the large intervening interstellar absorption, ROSAT is only sensitive to the very high energy part of the X-ray spectrum. Subtle changes in the shape of the X-ray energy distribution may overwhelm any other bulk bolometric variations. Therefore, as long as the photometric light curve and its colour behaviour is not known with accuracy, the 'Her X-1' model for RX J0925.7–4758 should only be considered as a working hypothesis. If this interpretation is correct, then $K_X \geq K_{HeII} \approx 84$ kms^{-1} and the long orbital period point at a rather massive mass donor star. We show in Fig. 3 the possible relationships between the masses of the two components of RX J0925.7–4758. Very high inclinations would produce X-ray eclipses which are not observed. However, if the X-ray source is not compact or the X-ray eclipse narrow enough to have been missed in our data, this latter constraint may be somewhat relaxed. For $M_X = 1$ $M_\odot$, all non eclipsing solutions imply a companion more massive than the X-ray source as would be expected if thermally unstable Roche lobe overflow were the mass transfer mechanism driving the binary (van den Heuvel et al. 1992). Assuming $i \geq 30°$, the companion star may have a mass in the range of 1 to ≥ 3.5 $M_\odot$ and a radius in the range of 5 to 8 $R_\odot$. This range of values is fully consistent with the giant or subgiant A0 to K4 star inferred from the absence of visible stellar signatures in the optical spectrum. Non eclipsing solutions with companion stars less massive than the X-ray source are allowed if one uses the H_α velocities instead. However, February 1994 and April 1992 data (MHP94) both suggest that the amplitude of the He II $\lambda 4686$ radial velocities is indeed larger than that of H_α.

It is well known that the velocity dispersion of local disk populations of stars increases with age (Wielen 1977). Although the scattering mechanism is still controversial, it results in an increasing scale height with stellar age. If the mass of the companion star in RX J0925.7–4758 is larger than 2 $M_\odot$, then the system cannot be much older than 1.2 10^9 yr (e.g. Schaller et al. 1992). Such relatively young populations have a rather small scale height of ≈ 200 pc (e.g. Robin & Crézé 1986). Objects like RX J0925.7–4758 may thus exhibit a strong concentration towards the galactic plane which would explain the scarcity of their detections so far.

Finally, we note that although the high mass transfer episode of RX J0925.7–4758 may have started in the giant-subgiant state, the evolved phase is still long enough ($\approx 10^8$ yr) to substantially increase the mass of the accreting white and drive it over the Chandrasekhar limit.

5 Summary

New spectroscopic and photometric observations show that the orbital period of RX J0925.7–4758 is in the range of 3.55 - 4.03 d . This is the longest orbital period known for supersoft sources if one excludes the symbiotic systems. In order to fill its Roche lobe, the mass donor must be slightly evolved, and the absence of detectable stellar absorption features in the optical spectrum argues in favour of an A0 to K4 giant or subgiant star. A 4.1 day long ROSAT HRI monitoring suggests that the X-ray flux of RX J0925.7–4758 varies with orbital phase. If the He II λ4686 radial velocity reflects the motion of the X-ray source then the mass donor star may be more massive than the accreting white dwarf. However, this conclusion depends on the validity of the 'Her X-1' model for RX J0925.7–4758 which cannot yet be firmly established from the available observations.

Acknowledgement: This work is based on observations obtained at the European Southern Observatory, La Silla, Chile with the ESO-Dutch 0.9 m and the ESO 1.5 m telescopes. We are especially grateful to Dr. S. Mottola who kindly carried out the optical photometric observations in June 1994. We also thank M. Pakull for useful discussions and for critical reading of this manuscript. The ROSAT project is supported by the Bundesministerium für Bildung, Wissenschaft, Forschung und Technologie (BMBF/DARA) and the Max-Planck-Gesellschaft. C.M. acknowledges support from a CNRS-MPG cooperation contract and thanks Prof. J. Trümper and the ROSAT group for their hospitality and fruitful discussions.

References

Beuermann K., Reinsch K., Barwig H., et al., 1995, A&A, 294, L1
Cowley A.P., Schmidtke P.C., Crampton D., Hutchings J.B., 1990, ApJ 350, 288
Dworetsky M.M., 1983, MNRAS 203, 917
Ebisawa K., Asai K., Dotani T., Mukai K., Smale A., 1996, in Röntgenstrahlung from the Universe, Eds. H.U. Zimmermann et al., MPE Report 263, p. 133
Gerend D., Boynton P.E., 1976, ApJ 209, 562
Kahabka P., 1996, A&A 306, 795
Lomb N.R., 1976, Ap&SS 39, 447
Motch C., Hasinger G., Pietsch W., 1994, A&A 284, 827 (MHP94)

Pakull M.W., Motch C., Bianchi L., Thomas H.-C., Guibert J., Ferlet R., Schaeidt S., 1993, A&A 278, L39
Robin A., Crézé M., 1986, A&A 157, 71
Scargle J.D., 1982, ApJ 263, 835
Schaller G., Schaerer D., Meynet G., Maeder A., 1992, A&ASS 96, 269.
van den Heuvel E.P.J., Bhattacharya D., Nomoto K., Rappaport S.A., 1992, A&A 262, 97
Wielen R., 1977, A&A 60, 263

The X-Ray Energy Spectrum of RX J0925.7–4758 with ASCA

K. Ebisawa[1], K. Asai[2], K. Mukai[1], A. Smale[1], T. Dotani[2], H.W. Hartmann[3], J. Heise[3]

[1] NASA/GSFC, Greenbelt, MD 20771 USA, and Universities Space Research Association
[2] Institute of Space and Astronautical Science, Yoshinodai, Sagamihara, Kanagawa, 229 Japan
[3] SRON Laboratory for Space Research, NL-3584 CA Utrecht, The Netherlands

Abstract. The super-soft X-ray source RX J0925.7–4758 was observed with the ASCA SIS with a superior energy resolution ($\Delta E/E \approx 10\%$ at 0.5 keV) for the first time. A simple blackbody model does not fit the data, and several absorption edges of highly ionized heavy elements are required. Introducing absorption edges significantly changes the best-fit blackbody parameters, such that the temperature is increased and the radius and bolometric luminosity are decreased. A massive white dwarf close to the Chandrasekar limit at a distance of $\gtrsim$ 10 kpc will be able to produce such an energy spectrum.

1 Introduction

Dozens of Super Soft Sources (SSS) have been discovered with Einstein and ROSAT (for a review, e.g., Hasinger 1994; Rappaport and Di Stefano 1996; Cowley et al. 1996; Kahabka and Trümper 1996). Steady nuclear burning on the surfaces of accreting white dwarves is a likely model for SSS (van den Heuvel et al. 1992; Heise et al. 1994). Observational information of SSS in the X-ray band is limited by spectral resolutions of the current instruments. While the ROSAT PSPC has a very suitable energy band (0.1 – 2 keV) for the study of SSS, its energy resolution ($\Delta E/E \sim 60\%$ at 0.5 keV) does not allow detection of local spectral structures such as emission lines or absorption edges.

Having a superior energy resolution ($\Delta E/E \sim 10\%$ at 0.5 keV), the ASCA Solid State Spectrometer (SIS) is potentially a powerful instrument for spectroscopic study of SSS, though its energy band (0.4 – 10 keV) is higher than the typical SSS energy range. RX J0925.7–4758 is an unusual SSS having most X-ray emission above 0.5 keV (Motch et al. 1993), and thus the most suitable target for the ASCA SIS.

The ROSAT spectrum of RX J0925.7–4758 is fit with the blackbody having $kT = 40 - 55$ eV with an inter-stellar absorption with $N_{\rm H} = (1.0 - 1.9) \times 10^{22}$ cm^{-2} (Motch et al. 1994). The large column density, which is consistent with the estimate from optical redenning of the continuum and strength of the interstellar absorption lines, suggests the source is located within or behind the Vela Sheet molecular cloud (d =425 pc) (Motch et al. 1994).

2 Observation and Data Analysis

RX J0925.7–4758 was observed in the ASCA AO3 phase, on December 22 1994, for 20 ksec.

2.1 Simple Blackbody Model Fit

Fig. 1 is the result of a blackbody plus inter-stellar absorption model fit. We used the interstellar absorption model by Morrison and McCammon (1983). In Tab. 1, we show best-fit parameters, although these parameters have little sense, since the fit is not acceptable at all (reduced $\chi^2 \sim 10$). There are two noticeable features. First, absorption edge-like features are seen at around 0.7, 0.9 and 1.4 keV. Second, although a significant amount of the hydrogen column density is required to account for the low energy absorption, the oxygen K-edge feature at 0.54 keV is much weaker than is expected for the interstellar medium having the cosmic abundance.

Table 1. Spectral parameters for the blackbody fit

Temperature	46 eV
Blackbody Radius	1.6×10^5 km (d/1 kpc)
$N_{\rm H}$	2.1×10^{22} cm^{-2}
Bolometric Luminosity	1.5×10^{40} (d/1 kpc)^2 ergs/s
χ^2/dof (dof)	10.0 (51)

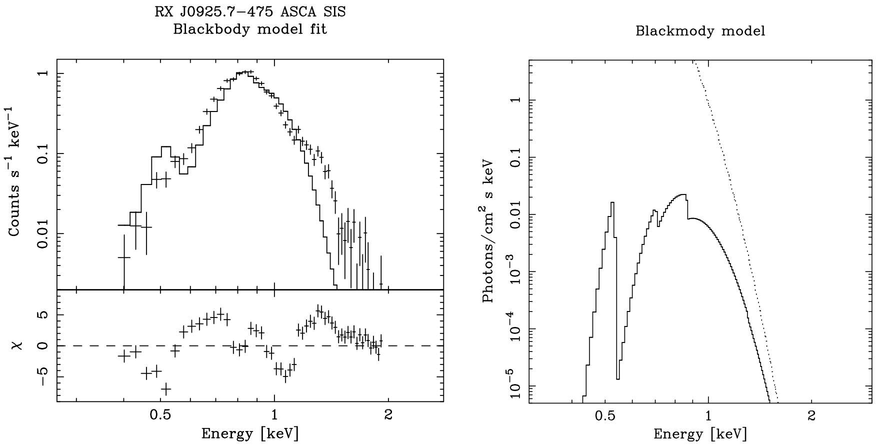

Fig. 1. Left: Blackbody model fit result. Right: the best-fit model with (solid-line) and without (dotted-line) the interstellar absorption.

2.2 Blackbody Model with Absorption Edges

Next we consider a simple model to fit the spectrum by introducing absorption edges to the blackbody model and changing elemental abundances of the intervening interstellar medium. We discuss origin of the absorption edges in section 3.1. At least three absorption edges are required at 0.94 keV, 1.04 keV and 1.43 keV (Tab. 2). In addition, in order to explain the small oxygen edge feature, we needed to reduce the oxygen abundance of the interstellar medium. Furthermore, we found reducing iron abundance significantly improves the fit at around the 0.71 keV Fe-L edge. Note that the blackbody temperature significantly increases, and the bolometric luminosity and radius decreases, compared to the fit without absorption edges (Tab. 1).

Table 2. Fit with a blackbody plus absorption edges

Temperature	96±11 eV	
Blackbody Radius	$140\pm^{180}_{70}$ km (d/1 kpc)	
$N_{\rm H}$	$1.0 \pm^{0.08}_{0.06} \times 10^{22}$ cm^{-2}	
Bolometric Luminosity	$2.1 \pm^{5.3}_{1.3} \times 10^{35}$ $(d/1\ {\rm kpc})^2$ ergs/s	
Edge Energies and Optical depths	0.94±0.03 keV	0.65±0.24
	1.04±0.02 keV	1.19±0.23
	1.43±0.04 keV	1.2±0.6
Oxygen abundance (cosmic = 1)	$0.38\pm^{0.11}_{0.14}$	
Iron abundance (cosmic = 1)	$0.2\pm^{0.5}_{0.2}$	
χ^2/dof (dof)	1.02 (42)	

* Oxygen and iron abundances are relative to the cosmic abundance by Anders and Ebihara (1982), which gives 7.41×10^{-4} and 3.31×10^{-5}, for O/H and Fe/H respectively.

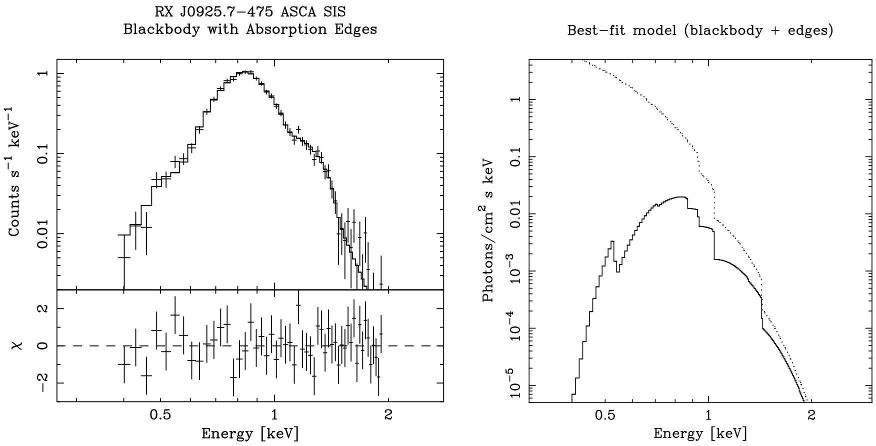

Fig. 2. Left: Fitting with a blackbody with absorption edges. Right: the best-fit model with (solid-line) and without (dotted-line) the interstellar absorption.

2.3 Application of a NLTE Spectral Model

We also tried a Non-Local Thermodynamical Equilibrium (NLTE) model by Hartmann and Heise (1996). They calculated the NLTE model spectral for two surface gravities, $\log g = 8.5$ and $\log g = 9.0$ (in the CGS unit). Effective temperatures are in the ranges of 5×10^5 to 8×10^5 K and 5×10^5 K to 10^6 K, respectively. In Fig. 3 and Tab. 3, we show results of the fitting with the $\log g = 9.0$ model. Oxygen and iron abundances for the interstellar medium were fixed to the values derived in the previous section.

Although the model fits the data well below the Ne IX K-edge (1.19 keV), the model predicts a much smaller flux above this energy. The Ne IX K-edge depth predicted in the model is much deeper than in the data, and the data rather indicates a higher energy edge feature which seems to correspond to the Ne X K-edge (1.36 keV). This indicates a higher ionization state is required than predicted by the present model.

Table 3. Spectral parameters with the NLTE model ($\log g = 9.0$) fit

Temperature	74 eV
Blackbody Radius	160 km (d/1 kpc)
$N_{\rm H}$	1.0×10^{22} cm^{-2} (fixed)
Bolometric Luminosity	9.7×10^{34} (d/1 kpc)^2 ergs/s
Oxygen abundance (cosmic = 1)	0.38 (fixed)
Iron abundance (cosmic = 1)	0.2 (fixed)
χ^2/dof (dof)	7.2 (51)

* The hydrogen column-density, oxygen and iron abundances are fixed to the values obtained in the previous section.

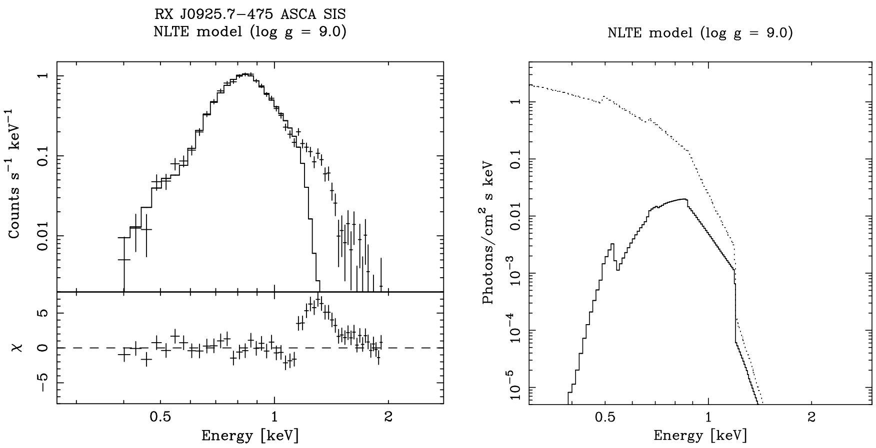

Fig. 3. Left: Fitting with the NLTE model by Hartmann and Heise (1996) for $\log g = 9.0$. Right: the best-fit model with (solid-line) and without (dotted-line) the interstellar absorption.

2.4 Comparison with the ROSAT Spectrum

ROSAT PSPC observation was carried out on November 20. 1992 (Motch et al. 1994). We obtained the PSPC data and responses of the same observation through two routes; one from Wouter Hartmann, which is based on the European ROSAT data analysis system, and the other from HEASARC at NASA/GSFC. For the latter, the off-axis mirror response was created with the program "pcarf". We found the normalizations of the two spectra differ by $\sim$ 30 % (HEASARC one is higher), although the spectral shapes are completely consistent. Origin of the normalization difference is under investigation.

In Fig. 4, we show the result of fitting the PSPC spectrum (taken from HEASARC) with the NLTE model by Hartmann and Heise (1996). Parameters are fixed to the best-fit values obtained with the ASCA SIS (table 3) besides the normalization. The normalization of the PSPC spectrum is 1.04 times that of ASCA, and the reduced χ^2 is 1.48 (dof=23).

Although energy resolution of the PSPC spectrum is not good enough to ascertain individual spectral edge features, systematic residuals are seen above $\sim$ 1.1 keV, suggesting the same high energy excess feature observed in the ASCA SIS spectrum. We conclude that the spectral shape has not changed systematically between the ROSAT PSPC and ASCA SIS observations which are 4 year apart. If the normalization of the HEASARC PSPC spectrum is correct, the luminosity does not show systematic variations either.

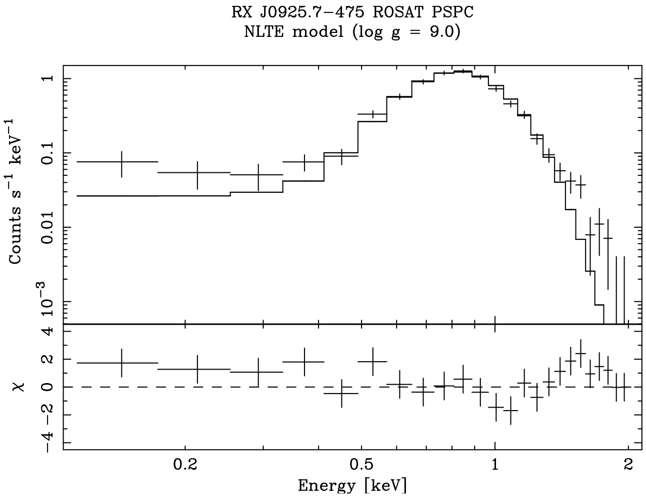

Fig. 4. Fitting the ROSAT PSPC spectrum (taken from HEASARC) with the NLTE model by Hartmann and Heise (1996) for $\log g = 9.0$. Parameters besides the normalization are fixed to those obtained with the ASCA SIS fit.

3 Discussion

3.1 Origin of the Absorption Edges

Let's consider origin of the observed absorption edges based on a simple model. If we assume the LTE condition, ionization balance is determined by the temperature, T, and the electron density, N_e, through the Saha relation. The electron density is of the order of the particle number density, and related with the temperature and the gas pressure as $P_g \approx N_e kT$. The gas pressure can be estimated from the hydrostatic equilibrium condition as $P_g \approx g/\kappa_R$, where g is the surface gravity and κ_R is the Rosseland mean opacity, ~ 0.4 cm^2 g^{-1}. Surface gravity of a white dwarf is typically 10^8 to 10^9 cm s^{-2}. Using the temperature obtained from the blackbody plus absorption edge model, ~ 96 eV, the typical electron number density in the atmosphere is estimated as $N_e \sim 10^{18}$ to 10^{19} cm^{-3}.

In Fig. 5, we show ion ratios for several abundant elements for $N_e = 10^{18}$ and 10^{19} cm^{-3}, as functions of the temperature. From this figure, considering the temperature is 90–100 eV, absorption edges which locate in the energy range 0.4–2.0 keV and may account for the observed spectral features will be the following: K-edges of O VIII (0.88 keV), Ne IX (1.19 keV), Ne X (1.36 keV) and Mg XI (1.75 keV), and L-edges of Fe XVII to $\sim$ Fe XXII (1.27 to $\sim$ 1.77 keV). Note that carbon and nitrogen are considered almost completely ionized.

The edge energies obtained through the blackbody plus absorption edge model fit (Tab. 2) do not precisely coincide these real edge energies. This is probably because (1) the continuum is not a blackbody shape and (2) the spectral features at the edges cannot be represented with the standard photoionization whose cross-section is proportional to E^{-3} above the edge. As a matter of fact, the model atmosphere spectrum (Fig. 3) indicates the continuum is represented with a combination of power-law spectra having discontinuities at edges. With these uncertainties, we may consider that the two apparent edges at 0.94 ± 0.03 keV and 1.04 ± 0.02 keV are due to the presence of O VIII (0.88 keV) and/or Ne IX (1.19 keV) edges. Note that the presence of Ne I edge at 0.86 keV due to the heavy interstellar absorption makes it difficult to ascertain the O VIII edge. The observed edge at 1.43 ± 0.04 keV is considered to correspond to the Ne X edge at 1.36 keV, although effects of the iron L-edges will not be negligible.

We tried a NLTE model by Hartmann and Heise (1996). Although the model could fit the data below the Ne IX edge at 1.19 keV, the strong Ne IX edge predicted by the model was not observed and significant residuals remain above this energy (Fig. 3). The data rather indicates presence of the Ne X edge, suggesting a higher ionization state. If the temperature is increased in this model, however, strong "emission edges" emerge in lower energies (see C VI and N VII edges at 0.49 keV and 0.67 keV respectively in Fig. 3 right), which do not fit the data. Such emission edges are caused by the outer temperature inversion layer, and it is known that temperature structure in the NLTE atmosphere is very sensitive to even small amounts of light metals (Li – Ca) (Rauch 1996). There will be more things to study in the NLTE model, and precise modeling of the ASCA spectrum is under progress.

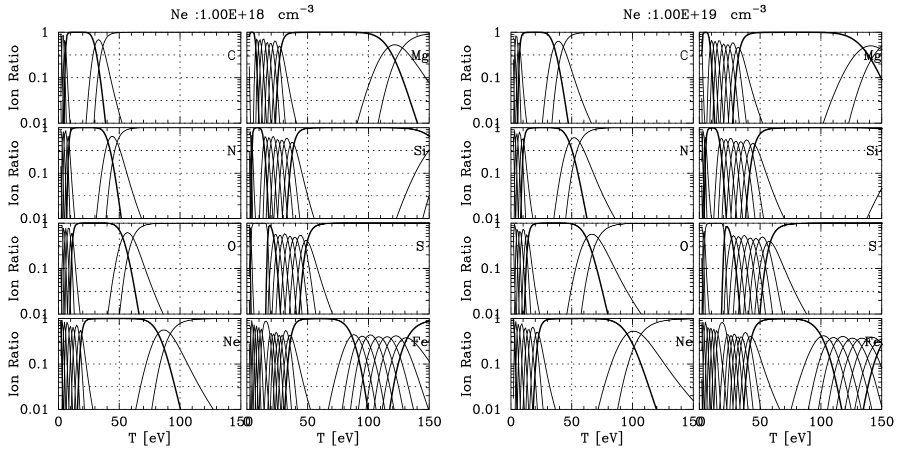

Fig. 5. Ion fractions for several elements determined from the Saha relation as functions of temperature. Shown for two electron densities, 10^{18} cm^{-3}(left) and 10^{19} cm^{-3}(right). Helium-like and Ne-like ions are shown with thick lines for each element.

3.2 A Model of RX J0925.7–4758

We found that the X-ray energy spectrum of RX J0925.7–4758 has several absorption edges of highly ionized heavy elements. Taking account of these absorption edges, the radius and the luminosity obtained from the blackbody model fit have become much smaller than those without assuming edges. Assuming the source is a white-dwarf, the minimum radius will be $\sim$ 3000 km at the Chandrasekar mass limit ($\sim 1.4 M_\odot$) (Fig. 6). For the radius obtained from the model fit (Tab. 2) to be consistent with the minimum white-dwarf radius, the distance will have to be $\gtrsim$ 10 kpc. Such a large distance will be consistent with a heavy interstellar absorption derived from the present fitting and optical observations (Motch et al. 1994). A high temperature ($\sim$ 96 eV) is required to account for the X-ray spectrum, and this is also consistent with a massive white-dwarf which can have such a high temperature (Tab. 2). Therefore, our conclusion is that RX J0925.7–4758 is a massive white-dwarf close to the Chandrasekhar limit at a distance of $\gtrsim$ 10 kpc.

References

Anders E., Ebihara M., 1982, Geochimica et Cosmochimica Acta 46, 2363
Cowley A.P., Schmidtke P.C., Crampton D., Hutchings J.B., 1996, in "Compact Stars in Binaries", ed. E.P.J. van den Heuvel & J. van Paradijs (Dordrecht: Kluwer) p. 439
Hasinger G., 1994, in "The Evolution of X-ray Binaries", ed. S.S. Holt and C.S.R. Day, AIP Conference Proceedings 308, p. 611
Hartmann H.W., Heise J., 1996, this volume p. 6
Heise J., van Teeseling A., Kahabka P., 1994, A&A 288, L45

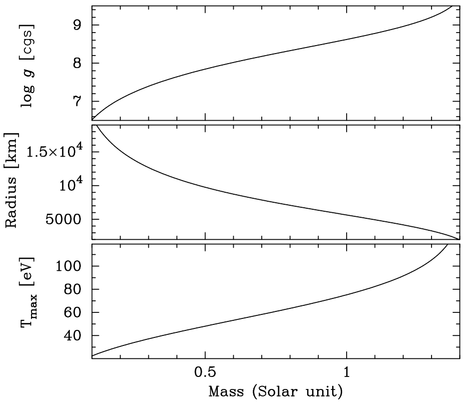

Fig. 6. Typical radius, surface gravity and the maximum temperature of a white dwarf as a function of the mass. The radius is derived from the formula by Pringle and Webbink (1975), and the surface gravity and the blackbody temperature corresponding to the Eddington limit are calculated.

Kahabka P., Trümper J., 1996, in "Compact Stars in Binaries", ed. E.P.J. van den Heuvel & J. van Paradijs (Dordrecht: Kluwer) p. 425
Morrison R., McCammon D., 1983, ApJ 270, 119
Motch C., Hasinger G., Pietsch W., 1994, A&A 284, 827
Pringle J.E., Webbink R.F., 1975, MNRAS 172, 493
Rappaport S., Di Stefano R., 1996, in "Compact Stars in Binaries", ed. E.P.J. van den Heuvel & J. van Paradijs (Dordrecht: Kluwer) p. 415
Rauch T., 1996, this volume p. 3
van den Heuvel E.P.J., Bhattacharya D., Nomoto K., Rappaport S.A., 1992 A&A 262, 97

Optical Photometry of RX J0019.8+2156 over the Last Three Years

T. Will, H. Barwig

Universitäts-Sternwarte München, Scheinerstr. 1, 81679 München, FRG

Abstract. We present time resolved UBVRI photometry of RX J0019.8+2156 which we performed with a multi-channel-photometer from 1992 to 1995. The light curves we received show regular and irregular brightness variations. Prominent cyclic depressions of 0.5 mag which cover a phase interval of 0.4 are interpreted as eclipses of a white dwarf by a Roche lobe filling secondary. Furthermore, a shallow minimum at phase 0.5 suggests a secondary eclipse. The orbital period derived from our light curves shows a little, but systematic difference to the most precise period value given in literature. The varying depth of the primary minimum as another phenomenon may be interpreted either as a cycle to cycle variation or as a quasi-periodic long term modulation.

1 Introduction

RX J0019.8+2156 (henceforth RX J0019) was discovered in the course of a search for soft X-ray sources (SSS) from the ROSAT All-Sky-Survey. It was the first candidate of SSS that has been found in our galaxy (Reinsch et al. 1993). Due to the relatively high apparent brightness (12.5 mag) of its optical counterpart this system provides the rare opportunity of studying these binary systems in further details. The first photometric and spectroscopic observations are described by Beuermann et al. (1995). Preliminary system parameters were derived from the optical data. Two models were suggested to describe the observational results. The first one assumes a pre-cataclysmic, detached binary system with two components containing one solar mass each. But this model explains neither the observed flickering nor the X-ray emission sufficiently. The second model transferring mass from a Roche-lobe filling secondary onto a White Dwarf primary at such a high rate that nuclear burning on its surface seems possible, is more likely. Due to the relatively long orbital period of 16 hours, which is commensurable with two days, observations have to cover extended time intervals in order to extract a mean photometric light curve. In the following chapters, the results from the observations over the last three years are presented.

2 Observations

The observations were performed by using the high speed multi-channel-photometer MCCP (Barwig et al. 1987) at the 80-cm telescope of the Wendelstein Observatory. This photometer allows us to monitor a programm star, a comparison star and the sky background simultaneously in UBVRI. By using this differential method, atmospheric transparency variations in particular during non-photometric nights can be taken into account. Our photometric data of RX J0019 covers 131 hours of observation within 25 nights which are spread over three years. The individual observing runs are listed in Tab. 1 (observations covering phase 0.0 are marked bold face).

Table 1. Journal of observations

Date of Observation	Start of measurement (HJD–2440000)	cycle (E)	duration (h)
21/09/1992	8887.296443	**0**	8.93
03/02/1993	9022.219093	**204**	3.28
07/02/1993	9026.240891	210	2.44
09/02/1993	9028.221953	213	2.91
11/02/1993	9030.233919	216	2.41
17/11/1993	9309.292191	638	4.78
06/12/1993	9328.245187	667	4.20
12/12/1993	9334.245408	676	2.01
16/12/1993	9338.201296	682	2.11
18/12/1993	9340.207739	685	6.45
28/12/1993	9350.196342	700	5.21
29/12/1993	9351.195015	702	4.42
09/01/1994	9362.237197	**719**	4.53
10/01/1994	9363.201174	720	5.36
11/10/1994	9637.339892	1135	8.22
12/10/1994	9638.299952	1136	3.46
13/10/1994	9639.252475	1138	7.16
14/10/1994	9640.412506	**1140**	6.23
15/10/1994	9641.301485	1141	3.21
16/10/1994	9642.299855	1142	3.65
18/10/1994	9644.266437	1145	8.44
20/10/1994	9646.283440	1148	6.77
21/10/1994	9647.284614	1150	5.52
22/10/1995	10013.224758	**1705**	10.16
23/10/1995	10014.249290	**1706**	9.31

3 Data Reduction

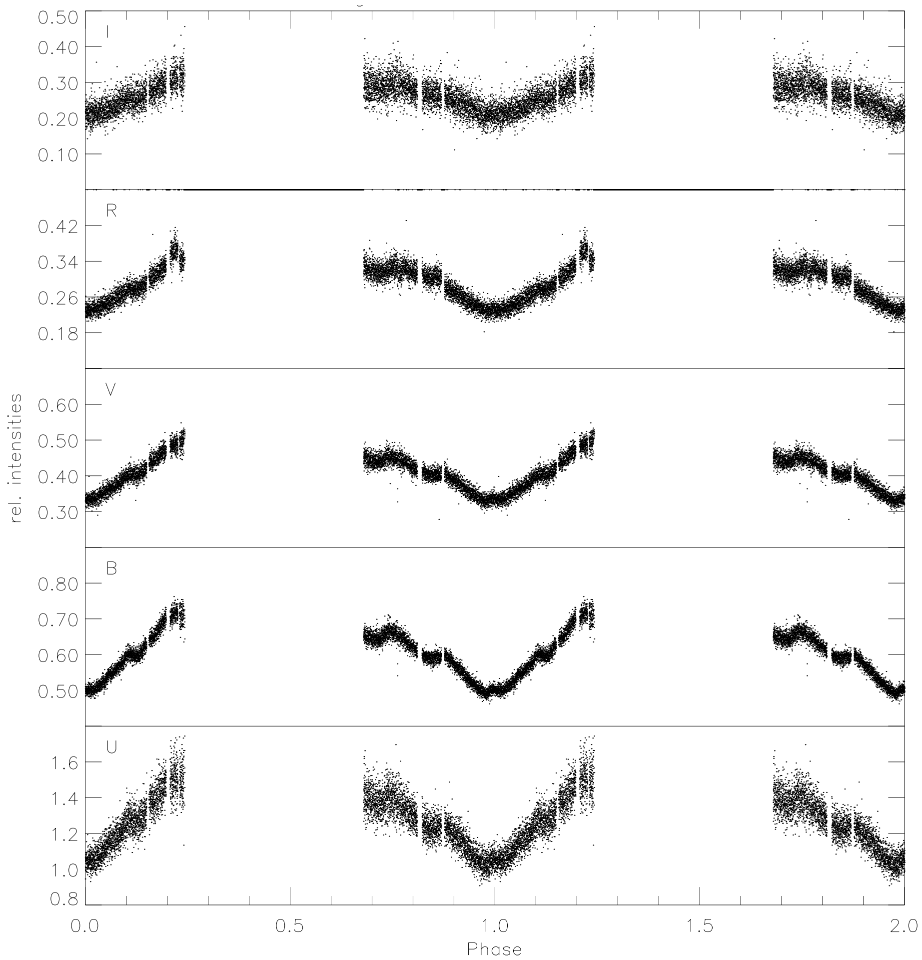

Fig. 1. Reduced light curves in UBVRI of September 21, 1992.

Usually, the original data of each channel is influenced by extinction and sky-background radiation. As the instrument measures simultaneously the brightness variations of a nearby comparison star as well as the sky straylight, these contributions can be eliminated by applying the so-called standard reduction procedure (see Barwig et al, 1987). In order to normalize the individual channels, calibration measurements were performed during photometric conditions by using the comparison star itself. The obvious constancy of the calibration coefficients during our observing campaign is indicative of a fairly high stability of all detectors. For this reason the observed non-periodic night-to-night variations of the light curves are very likely caused by instrinsic stellar variability of the X-ray binary system. The first reduced UBVRI light curves of RX J0019, which were also involved in the paper of Beuermann et al. (1995), are plotted in Fig. 1. They show a deep eclipse-like feature whose depth is dependent on the colour. The best S/N value was obtained in the B-filter, due to a combination of the instrumental quantum efficiency and the colour temperature of the target. Therefore, only B-light curves are displayed in the following figures.

4 Orbital Period

By examining our complete dataset, we could find only five light curves addition in which covered the phase of primary eclipse. The prominent deep eclipse features (see Fig. 2) were used to determine the orbital period of RX J0019. For this purpose, we fitted the light curves with a spline approximation assuming that the calculated zero points of their derivatives indicated the mid-time of the corresponding eclipses. As we used different spline parameters, we estimated the eclipse timing errors (see Tab. 2).

Table 2. Data used for period determination

cycle (E)	minima HJD–2440000 [d]	mean error [d]	O–C
0	8887.505	0.00071	0.00434
204	9022.250	0.00068	-0.00409
719	9362.382	0.00080	0.00683
1140	9640.457	0.00029	-0.00951
1705	10013.602	0.00067	0.01196
1706	10014.273	0.00085	0.00139

Applying a linear least-square-fit we received the ephemeris of the mid-eclipse time T_0:

$$T_0 = \text{HJD } 2448887.509(2)\text{d} + \text{E} \times 0.6604721(72)\text{d}$$

Our period value within the error bars coincides with the photometric and spectroscopic periods published by Beuermann et al. (1995). But obviously there is a systematic difference to the photometric period of Greiner and Wenzel (1995), which had been derived from photographic plates taken over a time span of 40 years (while investigating plates over more than 100 years) (see Tab. 3). Further studies are needed to decide whether a period change occured in the meantime or whether the definition of minima was incorrect, because only parts of the eclipse phase were covered by observation.

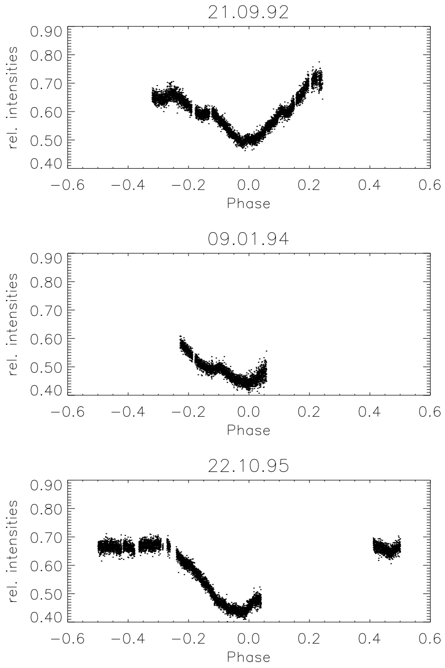

Fig. 2. Phase diagrams of all minima used for period determination (the phase was calculated from the period of Beuermann et al. 1995).

Table 3. Published orbital periods of RX J0019

Method	Period(error) [d]	Observations	Reference
photometry	0.66041(12)	Sep-Oct 92	Beuermann et al. (1995)
spectroscopy	0.66047(06)	Aug 92/93	Beuermann et al. (1995)
photometry	0.6604565(15)	1955–1993	Greiner et al. (1995)
photometry	0.6604721(72)	09/92–10/95	this paper

5 Combined Light Curves

In order to get a complete phase diagram of RX J0019, data of different nights had been combined. For this purpose only those measurements were selected which had been obtained under photometric conditions. During these nights the channel transformation coefficients could be determined at a high accuracy. Influences of instrumental instabilities on the light curves can be excluded applying the differential measuring method. In Fig. 3 (upper panel) two light curves obtained in 1992 and 1994, respectively, were combined with only a small

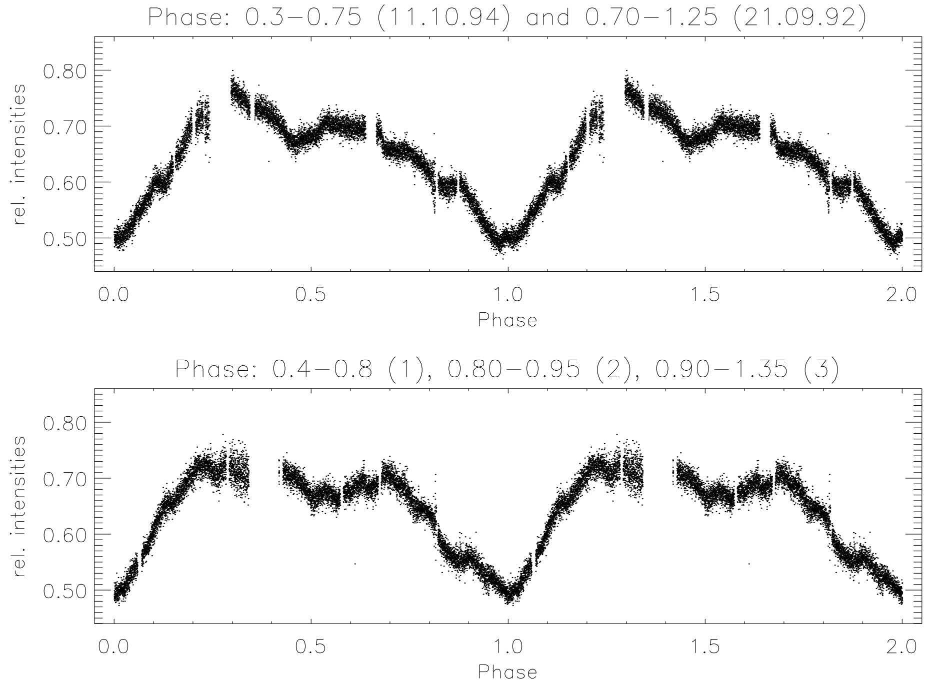

Fig. 3. Combination of light curves of different nights covering one complete orbital phase; in the lower plot the numbers in the brackets refer to the nights of December 18, 93, January 09, 94 and October 14, 94, respectively.

phase overlap. Their shape seems to be distorted by several step-like structures. Besides the most prominent primary eclipse feature, there is a significant depression at phase 0.5 suggesting a secondary eclipse. Gaps within the individual light curves are due to calibration measurements. In the lower plot of Fig. 3 another three light curves covering disjunctive phase intervals are plotted. The lightcurve also exhibits short-term variations which do not coincide with those of the corresponding phases of the upper plot while the phase of the secondary minimum has not changed significantly. In order to study the general photometric behaviour of RX J0019, all observational data within the time interval of three years were superimposed to a single phase diagram (Fig. 4). The individual short term variations obviously do not coincide with the orbital period and therefore disappear during superposition. Thus, only two eclipse features remain prominent. The appearance of a secondary minimum is of obvious discrepancy to the favoured model of RX J0019 for which an orbital inclination of 20 degrees is assumed. An interesting phenomenon hidden in the averaged phase diagram are the varying depths of the primary minima, plotted in Fig. 5. This variation may be approximated by a sine fit with a maximum period of 1.8 years. Another aspect is conspicious in this plot: minima of even cycles are brighter than those of odd cycles.

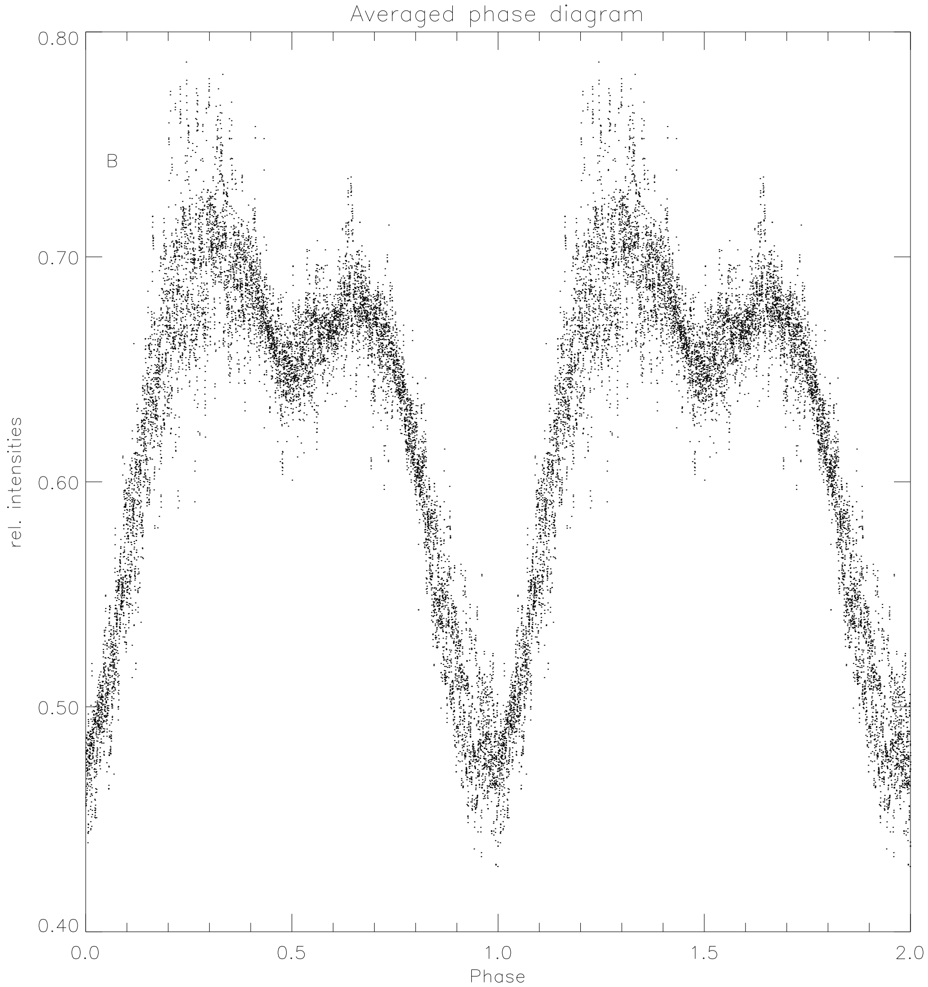

Fig. 4. Superposition of all light curves; the orbital phase is plotted twice.

Acknowledgement: The authors like to thank the staff of the observatory for their permanent efforts not to waste a single photon. They are also very grateful to S. Wolf for graphical processing of the plots.

References

Barwig H., Schoembs R., Buckenmayer C., 1987, A&A 175, 327

Beuermann K., Reinsch K., Barwig H., Burwitz V., deMartino D., Mantel K.H., Pakull M., Robinson E.L., Schwope A., Thomas H.-C., Trümper J., Zhang E., 1995, A&A 294, L1

Greiner J., Wenzel W., 1995, A&A 294, L5

Reinsch K., Beuermann K., Thomas H.-C., 1993, Astron. Ges. Abstr. Ser. 9, 41

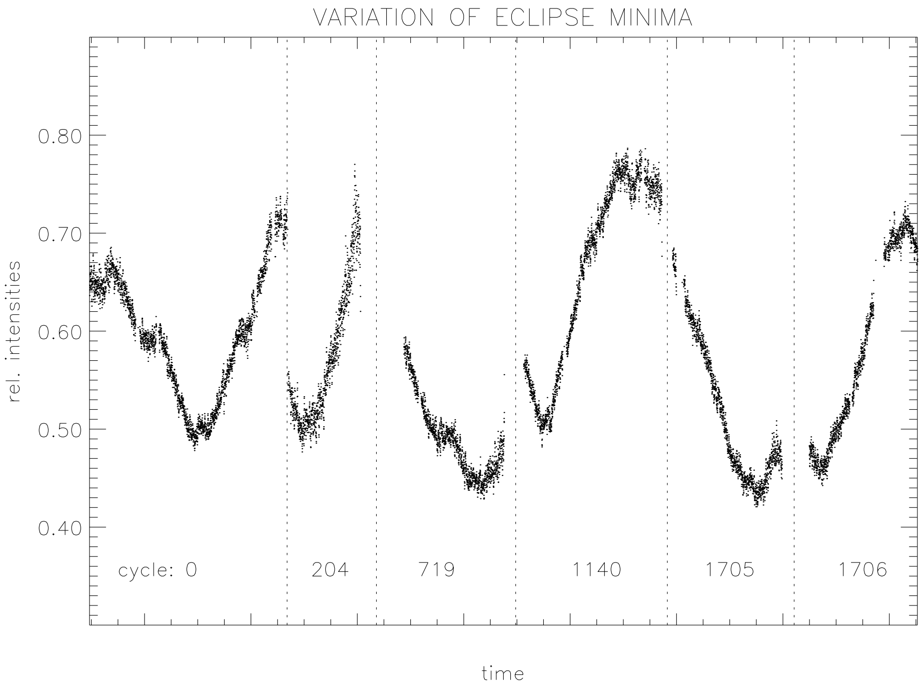

Fig. 5. Comparison of the depths of the primary minima. Each one is plotted in a seperate frame with its corresponding cycle number. Time interval between two tickmarks: 0.05 d

Phase Resolved UV Spectroscopy of RX J0019.8+2156

B.T. Gänsicke[1], K. Beuermann[1], D. de Martino[2]

[1] Universitäts-Sternwarte, Geismarlandstr. 11, 37083 Göttingen, Germany
[2] IUE Observatory VILSPA ESA, PO Box 50727, 28080 Madrid, Spain

Abstract. We present orbital phase-resolved UV spectroscopy of the supersoft X-ray source RX J0019.8+2156 obtained with IUE in 1992-93. The UV and optical light curves show a quasi-sinusoidal orbital modulation with wavelength dependent amplitude and a deep secondary minimum at $\Phi \sim 0.6$. The UV spectrum is of lower excitation than in other SSS. The various metal absorption lines are consistent with the source being located outside the gas layer of the galactic disc, though there is some evidence for intrinsic absorption. The UV spectrum of RX J0019 differs from those of the LMC sources CAL 83 and RX J0513.9–6951. A simple model where the UV light originates from the hot primary, the accretion disk and the heated secondary fails to reproduce the observed UV continuum.

1 Introduction

RX J0019.8+2156, henceforth RX J0019, is the only galactic supersoft source discovered from the ROSAT All Sky Survey at high galactic latitudes $|b| > 20°$ (Beuermann et al. 1995). In this paper, we will refer to supersoft sources (SSS) in the sense of close binaries containing an accreting, steadily burning white dwarf (van den Heuvel et al. 1992). Compared to the LMC SSS CAL 83 and RX J0513.9–6951 and to the only other galactic SSS known so far, RX J0925.7–4758, RX J0019 is optically brighter by ~ 5 mag and less absorbed by 1-2 orders of magnitude, underlining the potential of this object in understanding the physics of the SSS. RX J0019 shows variations of the optical, UV and X-ray flux as well as regular optical radial-velocity variations at a 15.85 hour period, interpreted as the binary orbital period (Beuermann et al. 1995). The moderately hot, irradiated accretion disc and the heated secondary star are expected to be the dominant sources of light at optical and UV wavelengths (Beuermann et

Table 1. Log of IUE observations.

Date	SWP spectra	LWP spectra	Orbital phase coverage
13/14 Jul. 1992	5	4	0.77-0.15
11 Jan. 1993	5	3	0.61-0.96
26-28 Aug. 1993	15	14	0.00-1.00

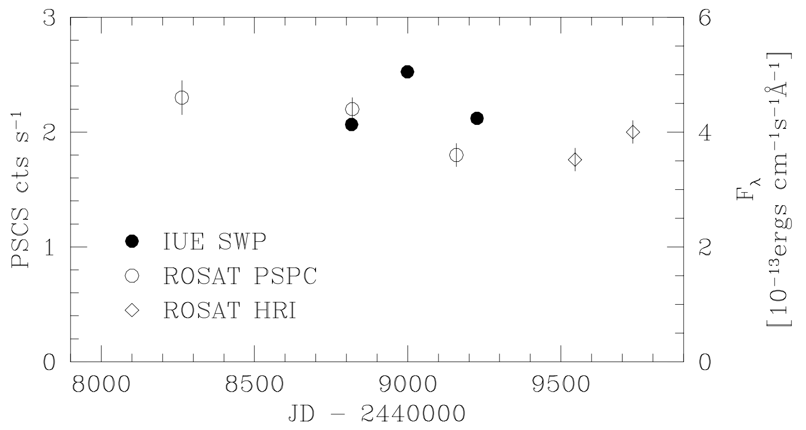

Fig. 1. UV and X-ray long term variability of RX J0019. The UV fluxes are averages over the SWP range (1250-1900Å), with statistical errors smaller than the point size. The ROSAT count rates are adopted from Reinsch et al. (1996a).

al. 1995). In addition to the orbital variability, the system shows erratic optical fluctuations of $\sim$ 0.5 mag on timescales of weeks to months as well as a quasi-periodic long term variability of $\Delta m_V \sim$ 1 mag with a cycle lengths of $\sim$ 40 years, interpreted as oscillations caused by intermittent hydrogen burning on the white dwarf. The current model (Beuermann et al. 1995, Greiner & Wenzel 1995) describes RX J0019 as an SSS with an accretion rate of $\sim 10^{-7}\,M_\odot$/yr, just a bit too low for stable hydrogen burning ($\sim 3 \times 10^{-7} M_\odot$/yr for a 1 $M_\odot$ white dwarf, Fujimoto 1982). The low X-ray luminosity of 4×10^{36}erg s^{-1} deduced from the ROSAT observations together with the optical brightness indicate that the system is momentarily in a low state.

2 Observations and Results

2.1 IUE Observations

UV observations of RX J0019 where carried out in July 1992, January 1993 and August 1993. A total of 25 SWP and 21 LWP exposures where acquired; full orbital coverage was achieved only in August 1993. Exposure lengths were typically 40 mins for the short wavelength range and 20 mins for the long wavelength range (Table 1). All spectra were obtained in the low resolution mode ($\sim$ 6 Å) and through the large aperture. All IUE images have been inspected for spurious features which have been removed.

The long-term variability of RX J0019 at UV and soft X-rays is shown in Fig. 1. The UV flux level of the January 1993 observations is $\sim$ 20% higher than in July 1992 and August 1993, whereas the X-ray observations show a variability of $\sim$ 35%. From the sparse data, it seems that the irregular fluctuations on timescales of weeks to months discovered by Greiner & Wenzel (1995) in the

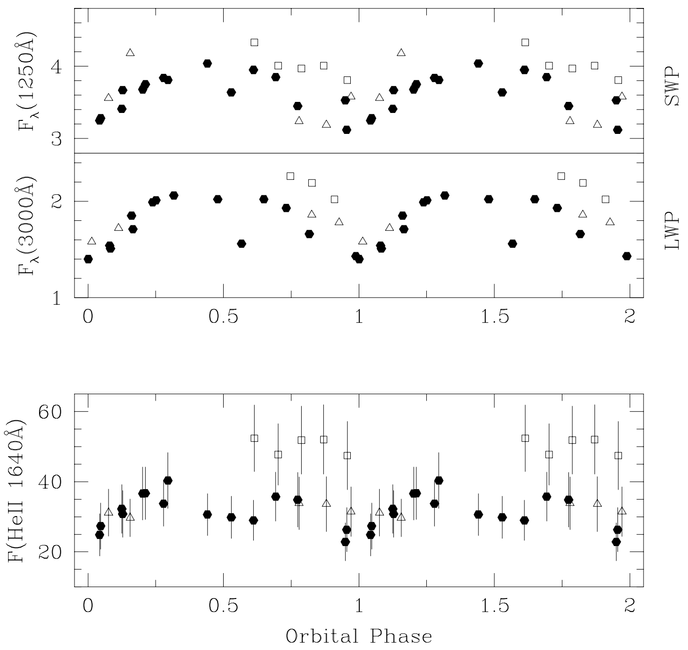

Fig. 2. UV light curves of RX J0019. Upper two panels: modulation of the continuum flux [10^{-13}erg cm^{-2}s^{-1}Å^{-1}] at far (1225–1275Å) and near (2950–3000Å) UV wavelengths. Statistical flux errors are smaller than symbol size. Bottom panel: modulation of the HeII λ 1640 line [10^{-13}erg cm^{-2}s^{-1}]. Errors are estimates from the uncertainty in defining the continuum. The individual IUE runs are coded as follows: △ July 1992, □ January 1993, ● August 1993. Data are shown twice for clarity.

optical are present also at other wavelengths. It is interesting to note that the optical magnitude measured with the FES of IUE was $V \sim 12.8$, both for the July 1992 and the January 1993 observations. Unfortunately no measure of the optical level with the FES could be performed in August 1993.

2.2 Orbital Variability

We derived light curves for the near (LWP) and far (SWP) UV continuum as well as for the HeII λ 1640 emission line. All spectra were dereddened with $E(B-V) = 0.1$ (sect. 2.3) and orbital phases were calculated according to the ephemeris of Greiner & Wenzel (1995). The line fluxes of HeII were measured by fitting a straight line plus a Gaussian emission line to the observed spectra in the region around 1640 Å. The definition of the continuum is prone to uncertainties, resulting in relatively large errors in the derived line fluxes. The orbital light curve shows a quasi-sinusoidal modulation with a broad minimum at phase 1.0

(Fig. 2). The depth of the modulation is declining towards shorter wavelengths (LWP: 32%, SWP: 22%), but reaches a maximum in HeII (43%). The three IUE runs show that in addition to the flux level, also the form of the light curve is subject to long term variations; the seasonal changes in the UV are especially strong in the HeII $\lambda\,1640$ line. Furthermore, the August 1993 data display orbit-to-orbit fluctuations of the UV flux, similar to those seen in the optical photometry of Beuermann et al. (1995). The most striking feature of the UV light curve of RX J0019 is the secondary minimum at $\Phi \approx 0.6$ seen in the August 1993 data. It was observed in both cameras, with smaller amplitude at short wavelengths (SWP: ~10%, LWP: ~25%). Recent photometry of RX J0019 (Will & Barwig 1996) reveals that the secondary minimum is present also at optical wavelengths, but that it is of highly variable nature.

2.3 The UV Spectrum

From the 2200 Å absorption in the observed LWP spectra a reddening of $E(B-V) = 0.10 \pm 0.03$ is derived, corresponding to $N_{\rm H} \approx 5 \times 10^{20}$ atoms cm^{-2} which is compatible to the absorption column determined from the ROSAT data (Beuermann et al. 1995) and to the galactic column density. Fig. 3 shows dereddened average spectra from the August 1993 run. The UV continuum of RX J0019 is characterised by a strong flux decline below 1600 Å and can be approximately described by a 19 000 K blackbody. This turnover is somewhat surprising for a system with presumably disc-dominated emission. The difference spectrum $(\Phi = 0.5) - (\Phi = 0.0)$ can be fitted by a 16 000 K blackbody. The only prominent UV emission line is HeII $\lambda\,1640$, indicating that the ionizing X-ray radiation in RX J0019 is of lower temperature than in the LMC SSS. At IUE resolution, no velocity variation is observed, limiting the radial velocity to ≤ 500 km/s.

Closer inspection of the IUE spectra of RX J0019 reveals a surprising multitude of absorption features. In Fig. 4 we compare average spectra from two different IUE runs. The similarity of these two spectra indicates that most of the observed features may be real. We identify a number of low ionization species (CI $\lambda\lambda\,1270$-88, CII $\lambda\,1335$, OI $\lambda\lambda\,1302$-06, SiII $\lambda\lambda\,1260/65$, 1304/09 and SII $\lambda\lambda\,1251/54/59$; note that the feature seen at ~1325 Å is due to a reseau mark). Table 2 lists the equivalent widths of the most prominent absorption features measured from the IUE spectra and compares them to the values expected for interstellar absorption at $d \approx 2$ kpc and $N_{\rm H} \approx 4 \times 10^{20}$ (compiled from Shull & van Steenberg (1985), van Steenberg & Shull (1988), Mauche et al. (1989), Burks et al. (1994) and Morton (1975, 1978)). The fact that some lines (e.g. SiII $\lambda\lambda\,1260/65$, MgII $\lambda\,2800$ and the complex around $\lambda = 1300$ Å) have equivalent widths much larger than what is expected from interstellar absorption and that they show an orbital variation of the equivalent widths is a strong indication that part of the absorption is intrinsic to the system. However, these metal absorption lines are much weaker than in hot (20 000-30 000 K) stellar atmospheres (e.g. Heck et al. 1984). In addition to the low-ionization species, the presence of several high ionization absorptions, e.g. NV $\lambda\lambda\,1238{,}43$ and SiIV $\lambda\lambda\,1394{,}1403$,

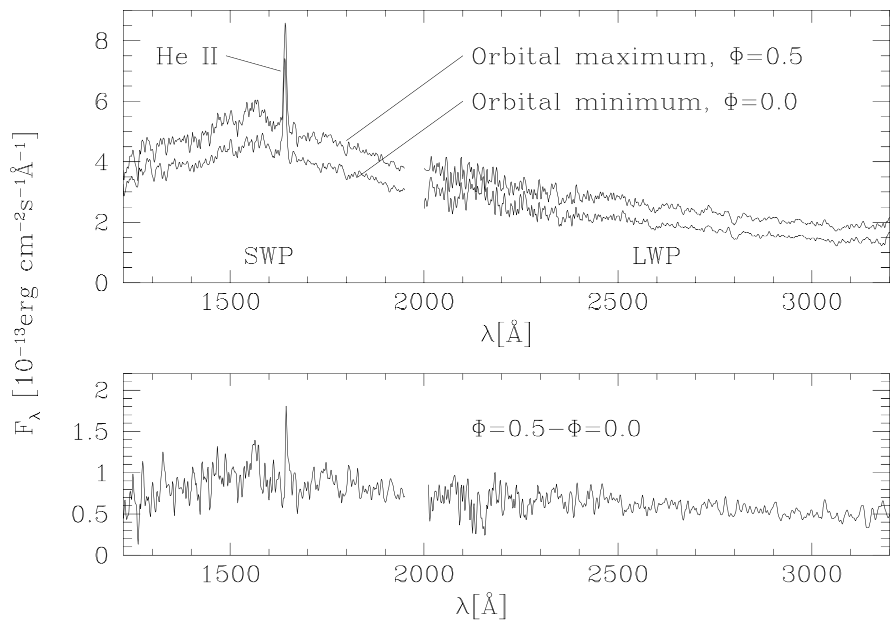

Fig. 3. Average UV spectra of RX J0019 in August 1993. Top: spectra at orbital maximum and minimum. Data have been dereddened with $E(B-V) = 0.1$. Bottom: difference spectrum orbital maximum minus orbital minimum.

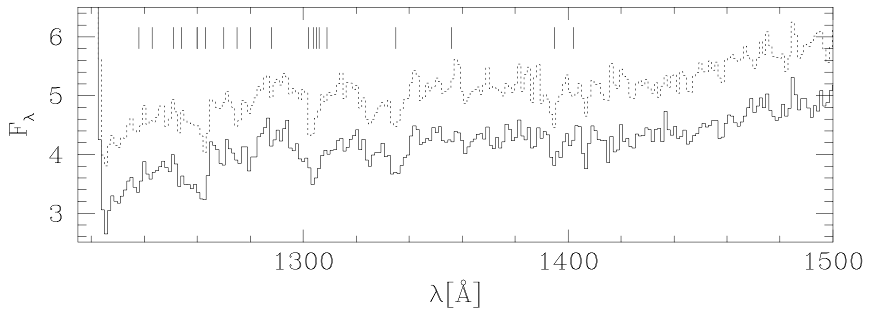

Fig. 4. Absorption features in RX J0019. Solid: average of the 15 spectra from August 1993. Dotted: average of the 5 spectra obtained in July 1992, shifted by one unit. The ticks show the positions of identified features (see text).

indicates intrinsic absorption (although these lines could be due to circumstellar absorption, e.g. Holberg et al. 1995). High resolution UV spectroscopy will allow to separate interstellar and intrinsic features and will also allow to constrain the system geometry from velocity variations of the intrinsic absorption.

Table 2. Equivalent widths [mÅ] of some absorption features as measured from the IUE spectra of RX J0019 and as expected by interstellar absorption.

λ [Å]	July 92	Jan. 93	Aug. 83	ISM
~ 1260	1400 ± 300	1700 ± 300	1850 ± 300 ($\Phi = 0.0$)	SiII, SII, CI.
			2550 ± 200 ($\Phi = 0.5$)	$\Sigma \approx 1150$
~ 1280	800 ± 200	500 ± 200	600 ± 200	CI ≈ 300
~ 1300	1300 ± 300	1600 ± 300	2700 ± 300 ($\Phi = 0.0$)	OI, SiII
			3500 ± 400 ($\Phi = 0.5$)	$\Sigma \approx 600$
~ 1335	1100 ± 200	1200 ± 200	1250 ± 200	CII ≈ 700
~ 1527	≤ 700	≤ 700	700 ± 200	SiII ≈ 500
~ 1560	600 ± 150	≤ 500	600 ± 150	CI ≈ 150
~ 1808	≤ 400	≤ 300	≤ 300	SiII ≈ 400
~ 2800	2600 ± 300	2200 ± 300	2850 ± 250 ($\Phi = 0.0$)	MgII ≈ 1000
			3450 ± 250 ($\Phi = 0.5$)	

3 Discussion

3.1 The UV Light Curve

From the radial velocity of the optical HeII lines and from the depth of the orbital modulation, Beuermann et al. (1995) derived an inclination of $i \approx 20°$ assuming that the optical modulation is due to the varying aspect of the secondary. Now, with the secondary minimum revealed, the light curve of RX J0019 looks reminiscent to that of CAL 87, a high-inclination system. There are, however, some important differences to note: Ingress and egress of the optical primary minimum (Beuermann et al. 1995) are less steep than in CAL 87, and the orbital modulation of RX J0019 ($\Delta m_{\rm V} \approx 0.5$ mag) is smaller than in CAL 87 ($\Delta m_{\rm V} \geq 1.5$ mag, Schmidtke et al. (1993)).

Recently, Schandl et al. (1996a,b) successfully fitted the optical light curve of CAL 87. Their model includes a heated secondary and an irradiated accretion disc with an illuminated high rim composed of cold, clumpy matter. This rim turned out to be an important ingredient to reproduce the observed light curve. Schandl et al. (1996a,b) applied their model also to the optical light curve of RX J0019, predicting $i = 60° - 70°$. It is, however, not clear if this model can explain the very deep secondary minimum with the obstruction of the secondary star by the accretion disc (rim).

Another problem concerns the X-ray observations of CAL 87 and RX J0019. The blackbody analyses of the ROSAT data of CAL 87 by Schmidtke et al. (1993) result in a high absorption column ($N_{\rm H} \sim 10^{22}$ atoms/cm^2) and low (observed) luminosity ($L_X \approx 10^{36}$erg s^{-1}), compatible with the model of Schandl et al. (1996a,b) where the central X-ray source is hidden from direct view. On the other hand, van Teeseling et al. (1996) show that the ROSAT observations of CAL 87 can be fitted with a hot, compact white dwarf. As for RX J0019, there is no sign for significant intrinsic absorption in the X-ray data.

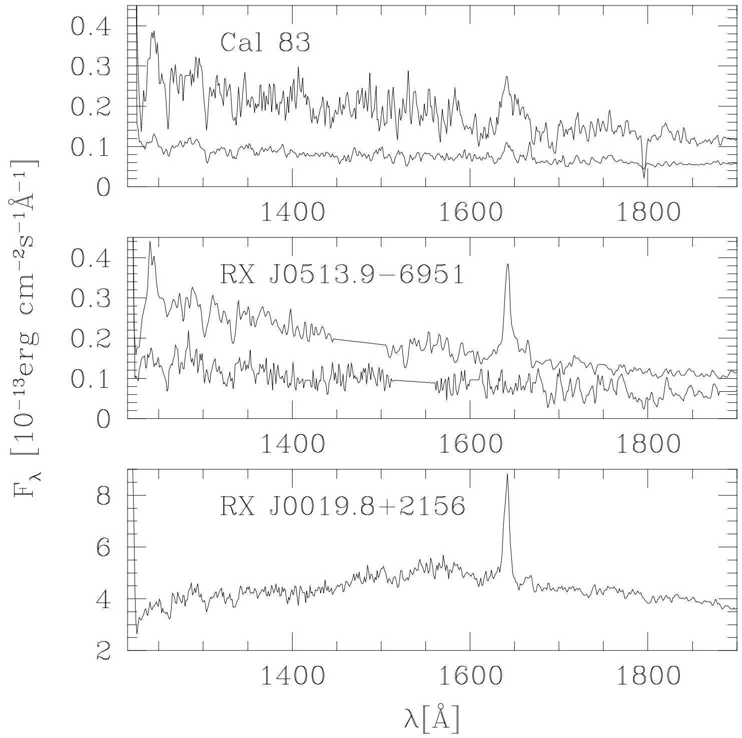

Fig. 5. UV spectra of CAL 83, RX J0513 and RX J0019. The spectra of CAL 83 have been discussed by Crampton et al. (1990) and Bianchi & Pakull (1988), the high state spectrum of RX J0513 by Pakull et al. (1993). In the RX J0513 spectra, cosmic hits have been removed.

3.2 The UV Spectrum

In non-magnetic CV's with a high mass transfer rate (e.g. IX Vel, Long et al. 1994) the accretion disc is the dominant light source at short wavelengths, with a spectrum rising up to far UV wavelengths. In SSS, the hot (a few 100 000 K) and luminous ($\sim 10^{38}$erg s^{-1}) burning white dwarf should cause an additional heating of the accretion disc, resulting in a very blue continuum.

In Fig. 5, we compare all UV observations of SSS obtained so far. The LMC sources CAL 83 and RX J0513 have almost identical spectra, with a rising continuum as expected from a hot accretion disc. Furthermore, they exhibit UV high and low states with an amplitude of $\sim$ 50%, very similar to the variations observed at optical wavelengths (Reinsch et al. 1996b,c; Southwell et al. 1996). The main difference between the UV appearance of RX J0019 and the LMC sources is the flux turnover below 1600 Å and the lack of high excitation emission lines (e.g NV λ 1240). A reasonable fit for the spectrum at $\lambda \geq 1600$ Å can be achieved using the simple model for an irradiated accretion disc and secondary star described by Reinsch et al. (1996b,c) with the following parameters: $M_{\rm wd} = 1.0{\rm M}_\odot$, $M_{\rm sec} = 1.6{\rm M}_\odot$, $i = 20°$, $d = 2\,{\rm kpc}$, $L_{\rm wd} = 3.5 \times 10^{36}{\rm erg\ s}^{-1}$ and $\dot{M} = 10^{-8}{\rm M}_\odot/{\rm yr}$. These values should be considered only of indicative character as the model of a flat disc and the assumption of blackbody emission is surely to simple and as the inclination might be higher. However, it is evident that also at higher inclinations, a standard accretion disc with an $\dot{M}$ needed for stable burning ($\sim 3 \times 10^{-7}{\rm M}_\odot/{\rm yr}$) produces too much UV flux and can not reproduce the observed flux turnover. A speculative model that could account for these feature is a disc truncated in the inner, hot regions; e.g. by the magnetic field of the white dwarf.

Acknowledgment: We thank S. Schandl for interesting discussions about modeling the light curves and spectra of SSS. This work was supported in part by the DARA under project number 50 OR 9210.

References

Beuermann K., Reinsch K., Barwig H., Burwitz V., de Martino D. et al., 1995, A&A 294, L1
Bianchi L., Pakull M.W., 1988, in A Decade of UV Astronomy with IUE, p. 145
Burks G.S., Bartko F., Shull J.M., Stocke J.T., Sachs E.R., Burbidge E.M., Cohen R.D., Junkkarinen V.T., Harms R.J., Massa D., 1994, ApJ 437, 630
Crampton D., Cowley A.P., Hutchings J.B., Schmidtke P.C., Thompson I.B., Liebert J., 1987, ApJ 321, 745
Fujimoto M.Y., 1982, ApJ 257, 767
Greiner J., Wenzel W., 1995, A&A 294, L5
Heck A., Egret D., Jascheck M., Jascheck C., 1984, ESA SP-1052
Holberg J.B., Bruhweiler F.C., Andersen J., 1995, ApJ 443, 753
Long K.S., Wade R.A., Blair W.P., Davidson A.F., Hubeny I., 1994, ApJ 426, 704
Mauche C.W., Raymond J.C., Córdova F., 1988, ApJ 335, 829
Morton D.C., 1975, ApJ 197, 85 & 1978, ApJ 222, 863
Pakull M.W., Motch C., Bianchi L., Thomas H.-C., et al., 1993, A&A 278, L39
Reinsch K., van Teeseling A., Beuermann K., Thomas H.-C., 1996a, in Röntgenstrahlung from the Universe, ed. Zimmermann H.U., et al., p. 183
Reinsch K., van Teeseling A., Beuermann K., Abott T.M.C., 1996b, this volume p. 173
Reinsch K., van Teeseling A., Beuermann K., Abott T.M.C., 1996c, A&A (in press)
Schandl S., Meyer-Hofmeister E., Meyer F., 1996a, this volume p. 53
Schandl S., Meyer-Hofmeister E., Meyer F., 1996b, A&A (subm.)
Schmidtke P.C., McGrath T.K., Cowley A.P., Frattare L.M., 1993, PASP 105, 863
Shull J.M., van Steenberg M.E., 1985, ApJ 294, 599
Southwell K.A., Livio M., Charles P.A., et al., 1996, this volume p. 165
van den Heuvel E.P.J., Bhattacharya D., Nomoto K., Rappaport S.A., 1992, A&A 262, 97
van Steenberg M.E., Shull J.M., 1988, ApJS 67, 225
van Teeseling A., Heise J., Kahabka P., 1996, IAU Symp. 165, 445
Will T., Barwig H., 1996, this volume p. 99

Optical Spectroscopy of RX J0439.8–6809 and 1E 0035.4–7230

A. van Teeseling[1], K. Reinsch[1], K. Beuermann[1], H.-C. Thomas[2], M.W. Pakull[3]

[1] Universitäts-Sternwarte Göttingen, Geismarlandstr. 11, 37083 Göttingen, Germany
[2] Max-Planck-Institut für Astrophysik, Postfach 1603, 85740 Garching, Germany
[3] Observatoire de Strasbourg, URA 1280 du CNRS, F-6700 Strasbourg, France

Abstract. We have identified RX J0439.8–6809 with a very blue $B = 21.5$ object. We find no evidence for X-ray or optical variability. The optical spectrum of RX J0439.8–6809 does not show any absorption or emission features, and suggests that the optical flux is the Rayleigh-Jeans tail of the soft X-ray component. RX J0439.8–6809 may be a short-period accreting binary or a $\sim 1 M_\odot$ post-AGB star.
We also present phase-resolved optical spectroscopy of the 4.1 hr binary supersoft X-ray source 1E 0035.4–7230. We detect strongly variable He II λ4686 emission and Balmer absorption lines. From radial velocity measurements we infer that a significant fraction of the hydrogen absorption lines originate on the donor star.

1 RX J0439.8–6809

1.1 Introduction

RX J0439.8–6809 has been discovered with ROSAT by Greiner et al. (1994). From the X-ray data they derived a blackbody temperature of $kT_{\rm bb} = 20 \pm 10$ eV and an absorption column density of $N_{\rm H} \sim 4 \times 10^{20}\,{\rm cm}^{-2}$, making RX J0439.8–6809 one of the softest supersoft X-ray sources. Its direction to the Large Magellanic Cloud, its absorption column, and the absence of objects brighter than $V \sim 19$ in the X-ray error circle indicated an LMC membership. Using the accurate X-ray position from a long-term monitoring campaign, we have identified RX J0439.8–6809 with a very blue and faint object. Here, we summarize the results of follow-up optical spectroscopy and photometry (Van Teeseling et al. 1996).

1.2 Optical Identification

From a long-term monitoring campaign with the ROSAT HRI we have obtained an average X-ray position of RX J0439.8–6809 with a statistical 1σ error of $\sim 2''$. The HRI X-ray position for epoch 2000 is: $\alpha = 4^h 39^m 49\overset{s}{.}6$, $\delta = -68°09'01''$. Figure 1 shows U and V images of the field containing RX J0439.8–6809 together with the X-ray error circle. There is only one object in the X-ray error circle (star 8 of Greiner et al. 1994), which we have identified with the optical counterpart of RX J0439.8–6809. This identification is supported by the extreme blueness of this faint object.

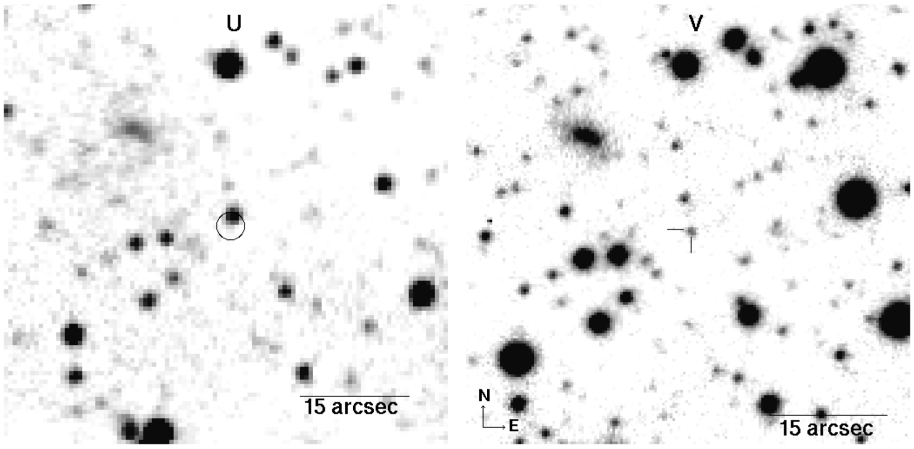

Fig. 1. U and V images of the field containing RX J0439.8–6809. The average HRI X-ray error circle with an error radius of 2″ is shown in the U image.

Using Landolt standard stars, we have determined the magnitudes of the optical counterpart: $V = 21.74 \pm 0.09$, $B = 21.50 \pm 0.04$, and $U = 20.40 \pm 0.10$. With $E_{B-V} = 0.1$ this gives: $V_0 \approx 21.4$, $(B-V)_0 \approx -0.3$, and $(U-B)_0 \approx -1.2$. If RX J0439.8–6809 is located in the LMC the absolute visual magnitude is $M_V \sim 2.9$.

1.3 Variability and Optical Spectrum

During our X-ray monitoring, the field of RX J0439.8–6809 has been observed almost weekly in B, V, and R with the Dutch 90 cm telescope at La Silla. Neither the X-ray light curve nor the optical light curves of RX J0439.8–6809 show significant variability. We can set a 3σ upper limit to the X-ray variability of $\sim 20\%$. To get a firm upper limit on the optical variability, we have obtained seven more B images with 10 min exposures at the 2.2m telescope at La Silla (Fig. 2), from which we can set a 3σ upper limit to the B variability of ~ 0.2 mag. The optical counterpart of RX J0439.8–6809 is also visible with apparently the same brightness as in 1995 on an ESO J plate taken in December 1975, which excludes strong variability on a time scale of 20 years.

In October 1995 we have obtained an optical spectrum of RX J0439.8–6809 with the 3.6m telescope at La Silla. The exposure was 6×30 min. The spectral resolution is ~ 6 Å per pixel (FWHM resolution of ~ 17 Å) and the wavelength range covered is 3750–6950 Å. The exposures were obtained during photometric conditions with a seeing of $\sim 1.5''$. The average flux-calibrated spectrum is shown in Fig. 3. The optical spectrum of RX J0439.8–6809 reveals a very blue continuum, from which we infer $V \sim 21.9$ and $B-V \sim -0.3$ consistent with the magnitudes inferred from our photometry. The optical spectrum has a blackbody

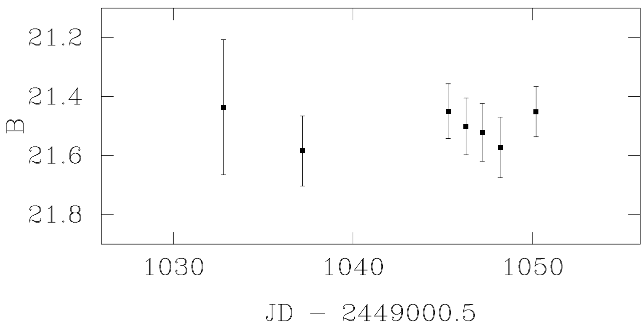

Fig. 2. The B light curve of RX J0439.8–6809 observed with the 2.2m telescope at La Silla.

temperature of $T_{\rm opt} \geq 10^5$ K and suggests that the optical flux is the Rayleigh-Jeans tail of a very hot spectral component. There are no detectable emission or absorption features in the spectrum. In particular, we do not find any evidence for the presence of He II λ4686 Å emission.

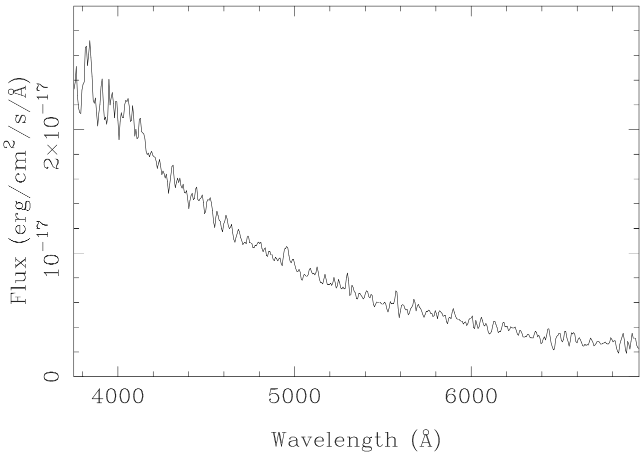

Fig. 3. Mean flux-calibrated spectrum of the optical counterpart of RX J0439.8–6809.

1.4 The Nature of RX J0439.8–6809

The intrinsic colours and absolute visual magnitude of the optical counterpart of RX J0439.8–6809 are not unusual for a low-mass X-ray binary (cf. Van Paradijs & McClintock 1995). However, it is difficult to hide a main sequence star in RX J0439.8–6809 which is sufficiently massive to drive steady or recurrent nuclear burning on a white dwarf (Van den Heuvel et al. 1992; Kahabka 1995).

If RX J0439.8–6809 is located in the LMC at a distance of ~ 50 kpc, the donor star has to be less luminous than approximately a G0 V star. If RX J0439.8–6809 contains an irradiated accretion disk, the absolute visual magnitude of RX J0439.8–6809 suggests a very short orbital period which would exclude a main-sequence donor star and support a helium-burning or degenerate donor star (Van Paradijs & McClintock 1994). However, a helium-burning star would probably be too luminous and a degenerate donor star may not be able to provide the necessary high accretion rate.

The optical faintness of RX J0439.8–6809, our strong upper limit on the variability, and the absence of He II λ4686 Å emission lead us to an alternative model. If we assume that the optical flux is the Rayleigh-Jeans tail of the soft X-ray component we can constrain the spectral parameters to a narrow range. Independent of whether we use a blackbody spectrum or a $\log g = 7$ LTE model atmosphere spectrum, we find an absorption column of $N_{\rm H} \approx 4 \times 10^{20}\,{\rm cm}^{-2}$, an effective temperature of $T_{\rm eff} \approx 270\,000$ K, a radius of $R \approx 5 \times 10^{9} (d/50{\rm kpc})$ cm, and a corresponding luminosity of $L \approx 1 \times 10^{38} (d/50{\rm kpc})^2\,{\rm erg\,s}^{-1}$. Figure 4 shows a blackbody spectrum and a $\log g = 7$ model atmosphere spectrum together with the optical spectrum and the defolded ROSAT spectra.

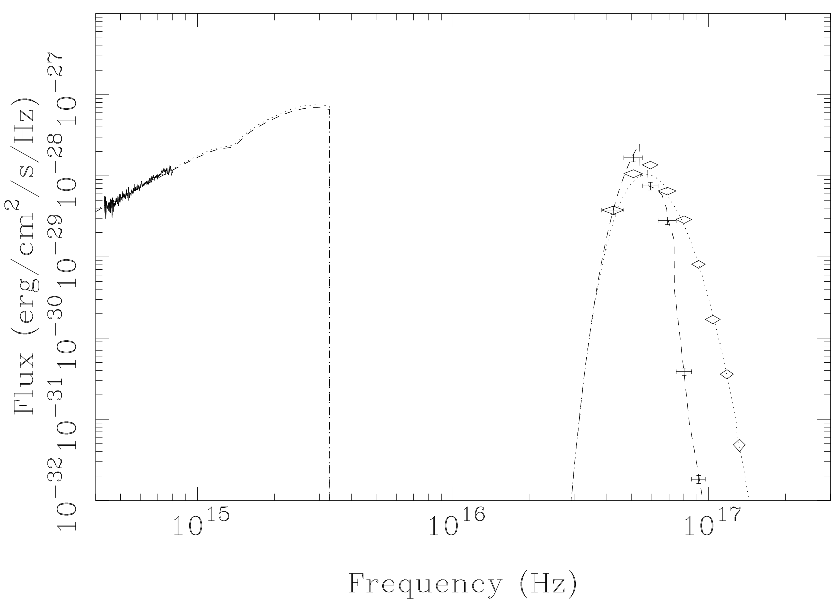

Fig. 4. The dashed line is the absorbed spectrum of a $\log g = 7$ LTE atmosphere with $T_{\rm eff} = 270\,000$ K and a metal abundance of 0.5 solar. The dotted line is an absorbed $T_{\rm bb} = 300\,000$ K blackbody spectrum. For both spectra $N_{\rm H} = 4 \times 10^{20}\,{\rm cm}^{-2}$. Also shown are the observed optical spectrum and the defolded X-ray spectrum of RX J0439.8–6809, using the blackbody spectrum (diamonds) and the model atmosphere spectrum (crosses).

The inferred spectral parameters are consistent with a $\sim 1 M_\odot$ star near the turn-over from the horizontal shell-burning track to the white-dwarf cooling track (e.g. Vassiliadis & Wood 1994). The evolutionary time scale of such a star would be of the order of a few years and would predict the existence of a planetary nebula around RX J0439.8–6809. However, no nebula could be detected around RX J0439.8–6809 (Remillard et al. 1995), which could be explained if RX J0439.8–6809 is suffering a late helium shell flash (e.g. Iben 1984) and has re-entered the high-luminosity quiescent helium-burning phase. It is unclear, however, whether the lack of variability is consistent with the evolutionary time scale of such a star.

2 1E 0035.4–7230

2.1 Introduction

1E 0035.4–7230 has been identified with a 20th mag variable blue star (Orio et al. 1994). Schmidtke et al. (1996) showed that 1E 0035.4–7230 undergoes nearly sinusoidal $\Delta V \sim 0.3$ variations on a period of ~ 4.1 hr. This orbital modulation is probably due to the changing aspect of the X-ray heated donor star. Schmidtke et al. (1996) also noticed the presence of weak variable He II λ4686 emission and an absorption feature at ~ 4868 Å. Here, we present some preliminary results of phase-resolved spectroscopy of 1E 0035.4–7230.

2.2 Phase-Resolved Spectroscopy

In October 1995 we obtained 12 spectra of 1E 0035.4–7230 with EFOSC1 at the 3.6m telescope at La Silla. Each spectrum has an exposure of 30 min, a spectral resolution of ~ 6 Å per pixel (FWHM resolution of ~ 17 Å), and covers the 3750–6950 Å region. We have minimized the loss of light due to differential atmospheric refraction by rotating the slit for each exposure perpendicular to the horizon. To obtain an accurate wavelength calibration, each spectrum was followed by a He-lamp observation with the telescope pointed to the same direction. Most exposures were obtained during photometric conditions with a seeing of $\sim 1.5''$. However, the flux-level of the average spectrum, which is shown in Fig. 5, is slightly reduced due to obscuring clouds during two exposures.

The average spectrum shows clear He II λ4686 emission and perhaps also weak He II λ5412 and O VI λ5291 emission. Surprisingly, Hβ is in absorption, but no other Balmer lines are visible in the average spectrum. Both the He II λ4686 emission and the Hβ absorption are strongly variable in strength and wavelength. In some individual spectra also the other Balmer lines are clearly in absorption (Fig. 5). The FWHM of the normalized average He II λ4686 and Hβ are ~ 18 Å and ~ 22 Å, respectively. Both average features are consistent with a narrow line which varies in wavelength. However, in some spectra the FWHM of Hβ seems to be significantly larger (see e.g. Fig. 5).

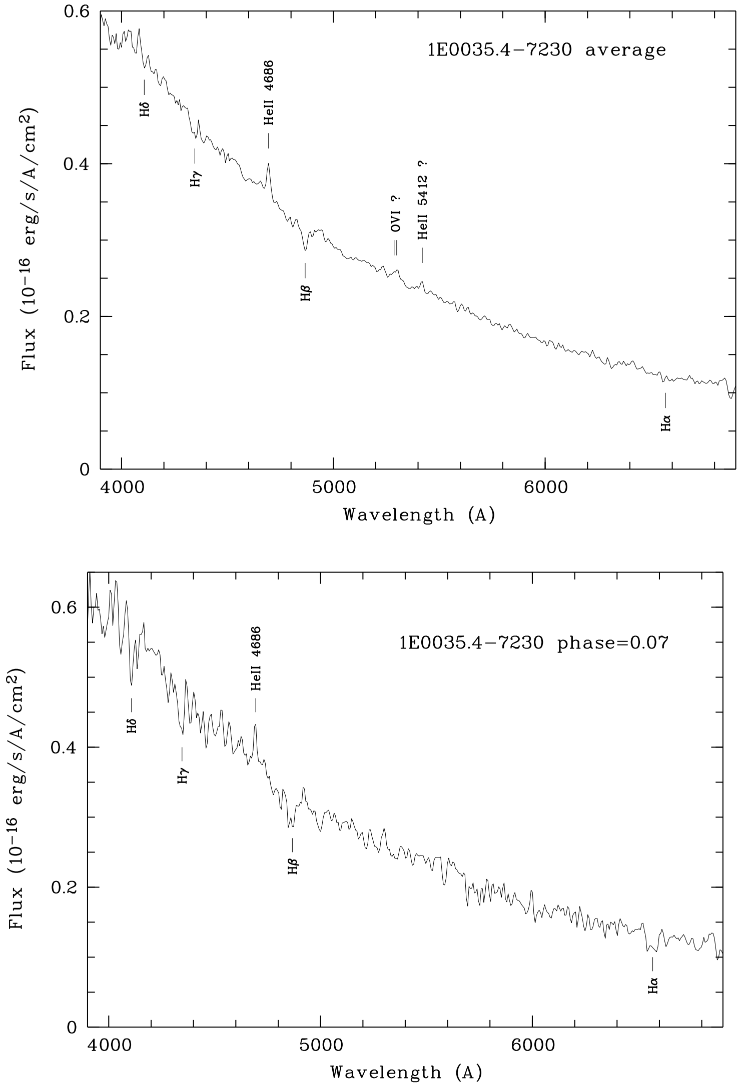

Fig. 5. Average flux-calibrated spectrum of 1E 0035.4–7230 (top panel) and flux-calibrated spectrum for photometric phase 0.07.

We have measured the radial velocity of He II λ4686 and Hβ in each of the 12 normalized spectra by cross-correlating the spectra with the normalized average spectrum and by fitting Gaussian profiles to the lines. Both methods give almost identical results. The He II λ4686 radial velocity is strongly variable, but we could not correlate this variability to the photometric phase. The Hβ radial velocity, however, can be fitted with a sine with the period fixed to the orbital pe-

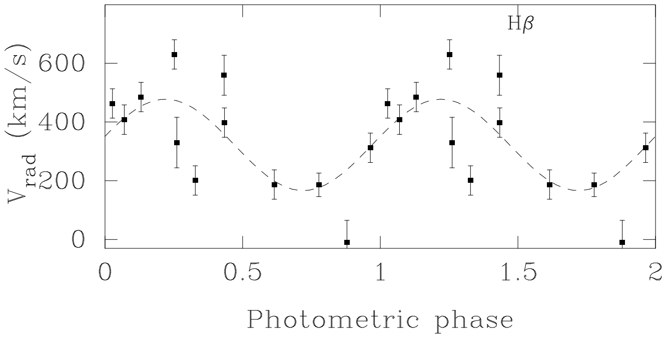

Fig. 6. Radial velocity of Hβ as a function of photometric phase. Each data point is plotted twice. The dashed line is a sine fit to the data.

riod. We have used the photometric ephemeris given by Schmidtke et al. (1996), where phase 0 corresponds to minimum optical light. Leaving the phase as a free parameter, we find a phase offset of the blue-to-red zero crossing compared to minimum optical light of only -0.03, and a coincidence probability of 4%. When one of the zero points of the sine is fixed to photometric phase 0, the probability of getting such a good fit with these data is only 0.5%. When the photometric modulation is due to the changing aspect of the X-ray heated donor star, the Hβ radial velocities imply that a significant part of the Hβ absorption originates on the donor star. However, the large FWHM of Hβ in some spectra suggests that the Hβ absorption is contaminated with a variable absorption component from the accretion disk. This would imply that the real radial velocity amplitude is larger than shown in Fig. 6. We also note that the mean velocity of Hβ is significantly higher than the mean SMC velocity.

2.3 Discussion

In a 4.1 hr binary with a white dwarf and a Roche-Lobe filling quasi-main-sequence star, the secondary star has to be a late K star or an M star. Using a white-dwarf luminosity of $5\,10^{36}\,\mathrm{erg\,s^{-1}}$, an $0.8 M_\odot$ white dwarf, and a donor star with the size of an M0 V star, we have calculated the temperature distribution on the surface of the donor star. The spectrum of the heated side of the secondary has been calculated by summing observed stellar spectra. The result depends on the amount of shielding by the accretion disk. Fig. 7 shows the calculated spectra for a flat disk and for an accretion disk with a half angular thickness of 10°. The observed photometric modulation and the average equivalent width of Hβ are consistent with a half angular thickness of $\sim 7°$. However, the model predicts much stronger Hγ and Hδ absorption. The weakness of Hγ and Hδ in the observed spectra may be due to a flatter temperature gradient in the irradiated atmosphere of the donor star (cf. Van Teeseling et al. 1994), or to a much redder spectrum of the heated side of the secondary.

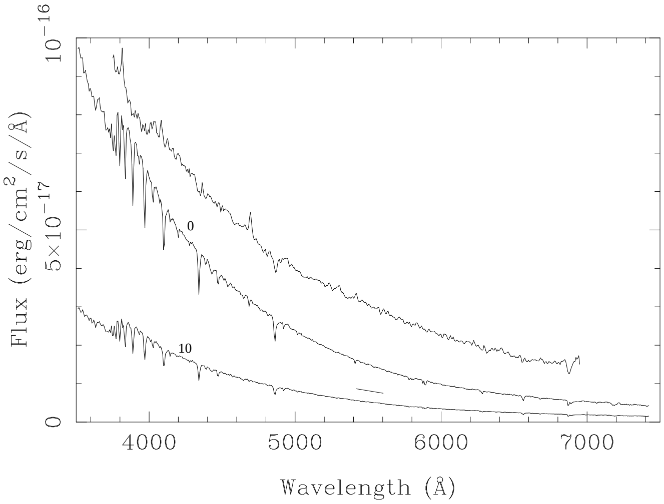

Fig. 7. Average spectrum of 1E 0035.4–7230 scaled to $V = 20.2$. The lower two spectra are the calculated spectra of the heated side of the donor star for no shielding by the accretion disk and for partial shielding by an accretion disk with a half angular thickness of 10°. The small line is the flux level of the heated side inferred from the photometric modulation of Δ V$\sim$0.3, assuming zero contribution at photometric phase zero.

Acknowledgement: This research was supported by the DARA under grant 50-OR 92 10.

References

Greiner J., Hasinger G., Thomas H.-C., 1994, A&A 281, L61
Iben I., 1984, ApJ 277, 333
Remillard R.A., Rappaport S., Macri L.M., 1995, ApJ 439, 646
Kahabka P., 1995, A&A 304, 277
Orio M., Della Valle M., Massone G., Ögelman H., 1994, A&A 289, L11
Schmidtke P.C., Cowley A. P., McGrath T.K., Hutchings J.B., Crampton D., 1996, AJ 111, 788
Van den Heuvel E.P.J., Bhattacharya D., Nomoto K., Rappaport S.A., 1992, A&A 262, 97
Van Paradijs J., McClintock J.E., 1994, A&A 290, 133
Van Paradijs J., McClintock J.E., 1995, in X-ray Binaries, W.H.G. Lewin et al. (eds.), Cambridge University Press
Van Teeseling A., Reinsch K., Beuermann K., 1996, A&A 307, L49
Van Teeseling A., Heise J., Paerels F., 1994, A&A 281, 119
Vassiliadis E., Wood P.R., 1994, ApJS 92, 125

Photometric Observations of Supersoft Sources in the LMC

P.C. Schmidtke, A.P. Cowley

Arizona State Univ., Dept. of Physics & Astronomy, Tempe, AZ, 85287-1504 USA

1 Introduction

The Magellanic Clouds are an ideal laboratory to study supersoft X-ray sources (SSS). The low-energy response of *ROSAT* detectors has offered an unprecedented opportunity to study the soft X-ray flux from objects with blackbody temperatures in the range $kT \sim 10 - 100$ eV. This radiation is only partially attenuated because interstellar absorption in the direction of the Clouds is low. Since the distance is known, properties of individual sources can readily be compared not only to models but also to each other. Furthermore, the LMC and SMC are sufficiently close that ground-based photometry and spectroscopy can be used to study the optical counterparts. As part of a program to identify SSS in the Clouds by their color and/or variability, UBV images of the fields of yet unidentified sources have been obtained with the 0.9-m telescope at Cerro Tololo Inter-American Observatory. Here we report the observations for two sources in the LMC: RX J0439.8–6809 and RX J0550.0–7151.

2 RX J0439.8–6809

CCD images of RX J0439.8–6809 were taken on 1995 November 29 under excellent seeing conditions and are presented in Fig. 1. The marked star corresponds to star #8 of Greiner et al. (1994) and has very blue colors ($V_{mean} \sim 21.6$, $B - V = -0.29 \pm 0.05$, $U - B = -1.25 \pm 0.10$). It is nearly coincident with the ROSAT HRI position given by van Teeseling et al. (1996), who have independently identified the same star as the optical counterpart.

To investigate the optical variability of this source, a set of 33 V images was taken over seven consecutive nights in 1995 November, yielding the light curve (on an instrumental scale) shown in Fig. 2. Variability, even within a single night, is apparent. We have tested the scatter of the observed magnitudes and concluded that the distribution of their deviations from the mean value greatly exceeds that expected from statistical errors alone. (The scatter of data for a nearby field star of similar brightness shows a normal distribution.) Although van Teeseling et al. (1996) found no variability greater than 0.2 mag in B, their measurements have much larger error bars, and individual observations were taken at widely spaced intervals (days or weeks apart).

Because RX J0439.8–6809 appears to vary on short time scale, we calculated a periodogram of the differential magnitudes for periods from 0.8 to 4 days. A portion of this periodogram is displayed in Fig. 3. The two strong peaks with periods near 0.1403 and 0.1637 days are one-day aliases of each other. Tests of the data set indicate that the shorter of these periods is significant with 90% confidence. Since at present we cannot discriminate between the two periods, a folded light curve for each is presented in Figs. 4 and 5. Both curves show a low-amplitude ($\Delta V \sim 0.15$ mag peak-to-peak), nearly sinusoidal variation with one maximum and one minimum through a cycle. Hence, the light curve for RX J0439.8–6809 closely resembles that of the supersoft source 1E 0035.4–7230 (Schmidtke et al. 1996), which is identified with a faint blue star in the SMC ($V_{mean} \sim 20.4$, $B-V=-0.15$, and $U-B=-1.06$). A comparison of the two sources shows the light curve for 1E 0035.4–7230 has a slightly larger amplitude (0.3 mag in V) and longer period (0.1719 days) than present in RX J0439.8–6809.

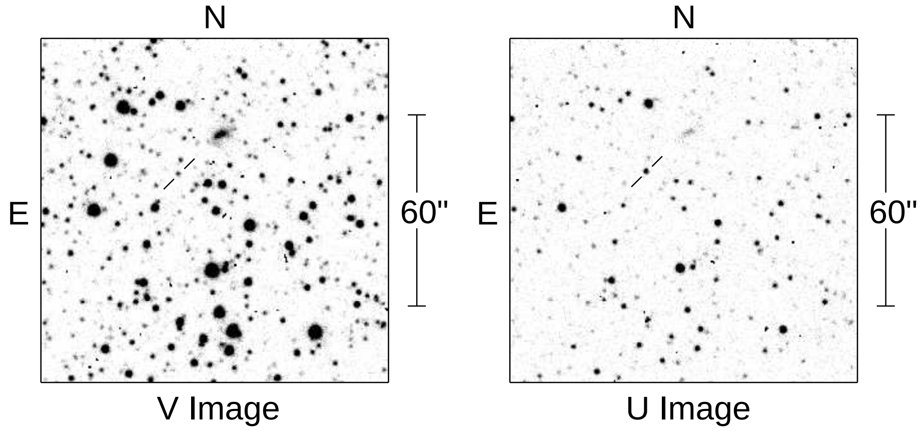

Fig. 1. V and B image of RX J0439.8–6809.

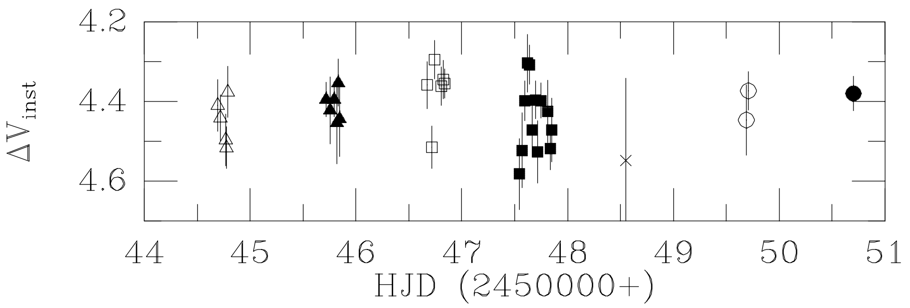

Fig. 2. V light curve for RX J0439.8–6809 in 1995 November.

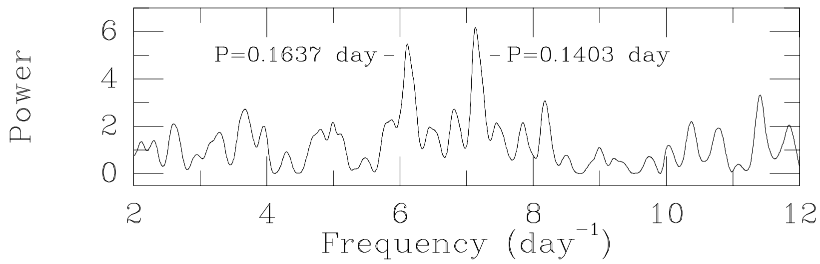

Fig. 3. Periodogram of V magnitudes for RX J0439.8–6809.

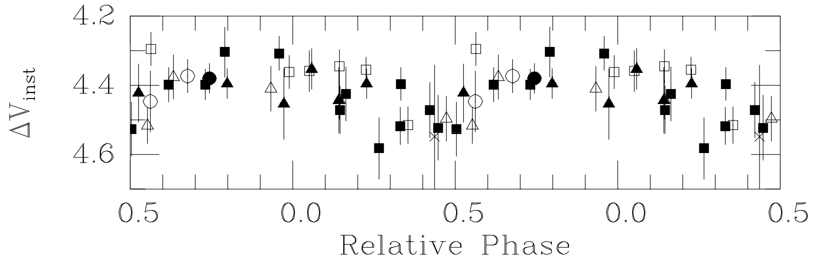

Fig. 4. V light curve for RX J0439.8–6809 folded on 0.1403 day period.

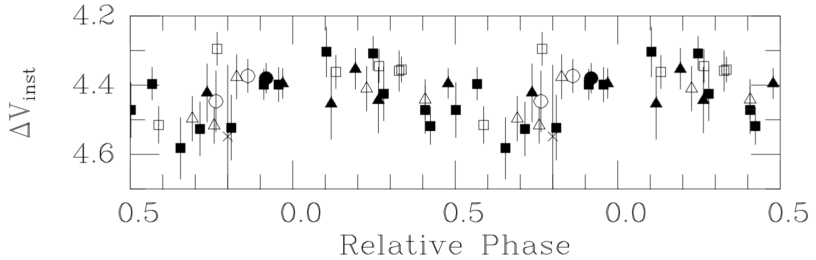

Fig. 5. V light curve for RX J0439.8–6809 folded on 0.1637 day period.

3 RX J0550.0–7151

RX J0550.0–7151 is a supersoft source in the LMC which was detected in the ROSAT PSPC field centered on CAL 87 (Cowley et al. 1993). Since RX J0550.0–7151 lies far off axis in the PSPC images, the point-spread function is extremely large, and the measured coordinates are poorly known. We obtained a well-centered HRI image in 1995, in which a weak source was present which we presumed was the supersoft source. At the HRI position there is a 13th magnitude star, which appeared to be the optical counterpart (Schmidtke & Cowley 1995). We subsequently have learned that in the ROSAT All-Sky Survey two close sources are present (Thomas 1996). These sources were not resolved in the early PSPC pointed observations. The HRI source for which we have found the optical counterpart is not the supersoft source, but rather the other, nearby X-ray source seen in the RASS data. Thus, we explicitly state that the optical counterpart of the supersoft source RX J0550.0−7151 has not yet been found, and this source is not present in either more recent PSPC nor in our HRI images, so it must be highly variable.

The source which we did detect should be referred to as RX J0549.8−7150. It has a HRI count rate of 0.008 sec^{-1} and coincides with a $V = 13.53$, foreground star. A CCD image of the field is shown in Fig. 6, with the HRI position indicated by a +. The measured colors ($B - V = +1.45$, $U - B = +0.86$) indicate a late-type star with a UV excess. Although it has been suggested that the source might be a symbiotic star or composite system, the colors are most similar to other ROSAT-selected dMe stars (see Schmidtke et al. 1994). Recently, Charles et al. (1996) reported that the spectrum of the optical counterpart has strong, narrow Balmer emission superposed on the spectrum of a cool star, in agreement with a dMe identification.

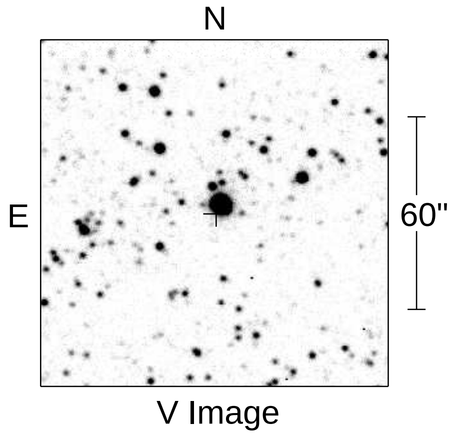

Fig. 6. V image of RX J0549.8–7150.

References

Charles P.A., Southwell K.A., O'Donoghue D., 1996, IAU Circ. 6305
Cowley A.P., Schmidtke P.C., Hutchings J.B., Crampton D., McGrath T.K., 1993, ApJ 418, L63
Greiner J., Hasinger G., Thomas H.-C., 1994, A&A 281, L61
Schmidtke P.C., Cowley A.P., Frattare L.M., McGrath T.K., Hutchings J.B., Crampton D., 1994, PASP 106, 843
Schmidtke P.C., Cowley A.P., 1995, IAU Circ. 6278
Schmidtke P.C., Cowley A.P., McGrath T.K., Hutchings J.B., Crampton D., 1996, AJ 111, 788
Thomas H.-C., 1996 (private comm.)
van Teeseling A., Reinsch K., Beuermann K., 1996, A&A (in press)

Optical Light Curve and Binary Period of the Supersoft X-Ray Transient RX J0513.9–6951

C. Motch, M.W. Pakull

CNRS, Observatoire de Strasbourg, 11 rue de l'Université, F-67000 Strasbourg

1 Introduction

The orbital period is a key parameter for our understanding of the dynamics and of the evolutionary status of contact binary systems. Steady-state hydrogen burning on the surface of a white dwarf requires accretion rates of few 10^{-7} $M_{\odot}$/yr which for main sequence stars can be reached if the donor stars masses are in the range of 1 - 3 $M_{\odot}$ and if the orbital periods lie between 8 h and 1.4 d (Rappaport et al. 1994). Much smaller orbital periods are possible, however, for *ex-nova* supersoft X-ray emitters in the constant-bolometric phase. The best-known case is GQ Mus which has P_{orb} = 85.5 min (Diaz & Steiner 1990). Orbital periods as long as ≈ 3.8 d may also exist if the mass donor star is slightly evolved (e.g. RX J0925.7–4758; Motch et al. 1994, Motch, 1996).

2 The Recurrent Supersoft Source RX J0513.9–6951

This LMC source (Schaeidt et al. 1993, Pakull et al. 1993) closely resembles the SSS prototype CAL 83 (P_{orb} = 1.04 d) in its X-ray - UV - optical luminosities and spectra, albeit with interesting differences. CAL 83 is a quasi-permanent X-ray source, but infrequently exhibits an optically bright state with exceptionally strong emission lines. Such an optical/UV spectrum is also displayed by RX J0513.9–6951, but here during the usual X-ray off state. However, there is some indication that the optical brightness *decreases* during X-ray outbursts (Pakull et al. 1993). Given their close resemblance one might expect similar masses and orbital periods for these two systems. From radial velocity measurements, Crampton et al. (1996) suggested an orbital cycle of 0.76 d, but their observations did not exclude alias periods near 0.32 and 0.43 d.

3 New Photometry

We have carried out CCD photometry of RX J0513.9–6951 during 6 consecutive nights from 1992 December 15 to 20 UT. We used the 90cm Dutch telescope located at ESO, La Silla, equipped with the RCA #5 CCD yielding a pixel size of 0.″51. CCD frames were acquired through a B filter with an integration time of 5 min. All CCD images were corrected for flat-field and bias using standard MIDAS procedures. After rejection of all images with seeing larger than 2.″5 a total of 103 frames remained. We performed differential photometry using a diaphragm of diameter 6.″2. The extraction area was chosen to be large enough to contain the faint companion located 1.″3 away from RX J0513.9–6951 (Crampton et al. 1996) and small enough to exclude light from the couple of stars located at 6.″9 in the north-east direction. We used as main comparison star the bright object located 50″ away from the X-ray source in the south-west direction. Our photometric calibration carried out in April 1992 (Pakull et al. 1993) gives B = 14.74 for this object. From the rms scatter of three other comparison stars with brightness similar to RX J0513.9–6951 we estimate that the error applicable to the differential photometry of RX J0513.9–6951 is ≈ 0.025 mag. The average brightness of B = 16.58 is consistent with our previous CCD photometry (Pakull et al. 1993) and with the magnitudes reported by Crampton et al. (1996) indicating that the system was optically bright and probably X-ray inactive at the time.

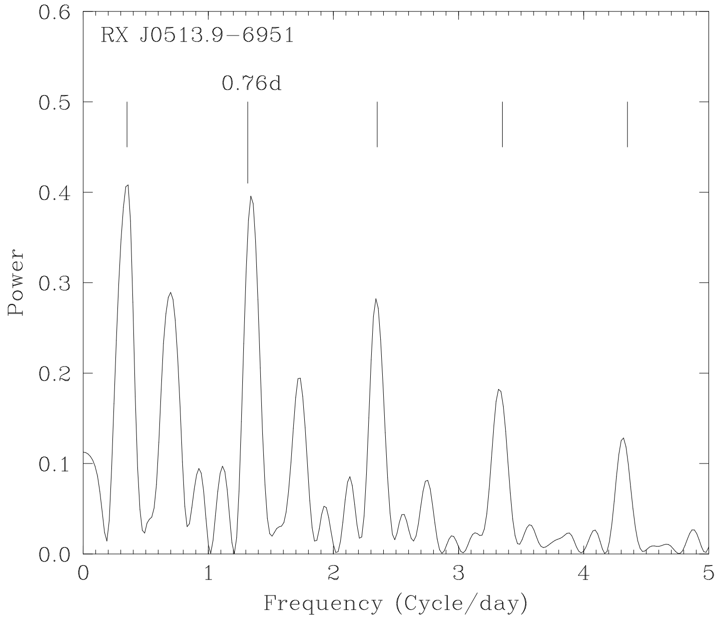

Fig. 1. Power spectrum of the B band data of RX J0513.9–6951. The 0.76 d orbital period proposed by Crampton et al. (1996) from spectroscopic data corresponds to one of the possible 1-day alias peaks.

A least square periodogram (Lomb 1976, Scargle 1982) of our B photometric time series is shown in Fig. 1. There are clear signatures of two sets of 1-day alias periodicities, the most significant one being coincident with that found by Crampton et al. (1996). The same set of alias is present in the minimum string length periodogram (Dworetsky 1983). No time series from any other secondary comparison star (or from seeing data) displays a similar signal. The relatively short length of the observing run and the small amplitude of the orbital modulation does not allow to constrain with large accuracy the best frequency. However, periods in the range of 0.745 ± 0.015 d are acceptable. Assuming a red noise distribution, we estimate at $\leq 10^{-4}$ the probability to find a power that strong at 0.745 d. The coincidence in period of our peak with with that reported by Crampton et al. (1996) (P = 0.76 d) is therefore interesting and in view of these results we conclude that the most probable orbital period is close to 0.76 d or one of its 1-day alias.

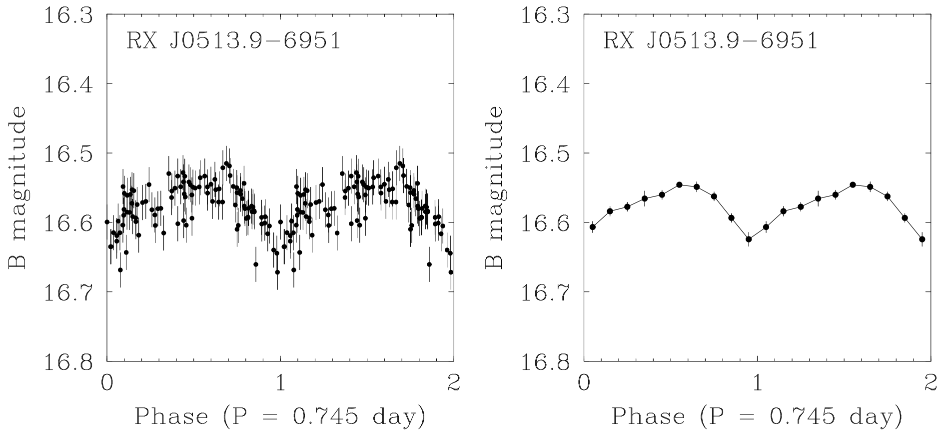

Fig. 2. B band photometric measurements folded with the best period of the periodogram. Time of phase 0.0 (minimum) is JD 2,448,971.737 ± 0.024. Left panel: individual data points. Right panel: averaged in 10 bins of phase.

The resulting light curve folded with a best period of 0.745 d is shown in Fig. 2. The full amplitude of the best fit sine wave is 0.059 mag. and the maximum range of variation is ≈ 0.1 mag. Although we note some intrinsic scatter, the light curve appears not to be perfectly sinusoidal, but shows some indication for a relative short phase ($\Delta\phi \approx 0.25$) of minimum light followed by a more gradual rise to maximum light.

4 Conclusion

The optical brightness of RX J0513.9–6951 shows a modulation of 0.1 mag amplitude with a period that is consistent with previously reported radial velocity variations. The light curve displays one relatively narrow minimum per cycle. So far it is not possible to determine the relative phasing between radial velocity and brightness. For the time being we therefore refrain from speculating on possible mechanisms that give rise to the orbital variations. Compared to the light curve of the twin source CAL 83 (Smale et al. 1988) the amplitude is smaller, in agreement with the probable lower system inclination of RX J0513.9–6951.

Acknowledgement: This work is based on observations obtained at the European Southern Observatory, La Silla, Chile with the ESO-Dutch 0.9-m telescope.

References

Crampton D., Hutchings J.B., Cowley A.P., Schmidtke P.C., McGrath T.K., O'-Donoghue D., Harrop-Allin M.K., 1996, ApJ 456, 320
Diaz M., Steiner J., 1990, Rev. Mex. Astron. Af 21, 369
Dworetsky M.M., 1983, MNRAS 203, 917
Lomb N.R., 1976, Ap&SS 39, 447
Motch C., Hasinger G., Pietsch W., 1994, A&A 284, 287
Motch C., 1996, this volume p. 83
Pakull M.W., Motch C., Bianchi L., et al., 1993, A&A 278, L39
Rappaport S., Di Stefano R., Smith J.D., 1994, ApJ 426, 692
Scargle J.D., 1982, ApJ 263, 835
Schaeidt S., Hasinger G., Trümper J., 1993, A&A 284 270, L9
Smale A.P., Corbet R.H.D., Charles P.A., Ilovaisky S.A., Mason K.O., Motch C., Mukai K., Naylor T., Parmar A.N., van der Klis M., van Paradijs J., 1988, MNRAS 233, 51

Non-LTE Model Atmosphere Analysis of the Supersoft X-ray Source RX J0122.9–7521

K. Werner[1], B. Wolff[2], M.W. Pakull[3], A.P. Cowley[4], P.C. Schmidtke[4], J.B. Hutchings[5], D. Crampton[5]

[1] Universität Potsdam, Lehrstuhl Astrophysik, Germany
[2] Universität Kiel, Institut für Astronomie und Astrophysik, Germany
[3] Observatoire Astronomique, Strasbourg, France
[4] Arizona State University, Department of Physics and Astronomy, Tempe, USA
[5] Dominion Astrophysical Observatory, Victoria, B.C., Canada

Abstract. The supersoft X-ray source RX J0122.9−7521 was discovered in the ROSAT all-sky survey and suspected to be a member of the Small Magellanic Cloud (Kahabka et al. 1994). More recently the source has been optically identified with an extremely hot PG 1159 star (Cowley et al. 1995).
Here we present a NLTE model atmosphere analysis of a pointed ROSAT observation combined with medium resolution optical spectroscopy. RX J0122.9−7521 appears to be the hottest known PG 1159 star. It is compact and relatively massive ($T_{\rm eff}$=180 000 K, log g=7.5, $M = 0.7\,{\rm M}_{\odot}$). In contrast to other stars of this group, the carbon and oxygen abundances in the helium-dominated atmosphere of RX J0122.9−7521 are unusually low. Our results allow a distance determination which clearly rules out SMC membership of RX J0122.9−7521.

1 Introduction

A distinct group of supersoft X-ray sources, the PG 1159 stars, comprises very hot hydrogen-deficient post-AGB stars. These stars represent an evolutionary transition phase between the central stars of planetary nebulae and the white dwarfs (WDs). Their masses are low ($M/{\rm M}_{\odot}$=0.5–0.9), and their effective temperatures and luminosities (and hence surface gravities) cover a fairly extended region in the HR diagram (see Fig. 6). Seven out of 27 known PG 1159 stars (including the object under discussion here) were detected with the ROSAT PSPC (see e.g. Werner 1996) and two of these appear in the ROSAT all-sky survey. All ROSAT detected PG 1159 stars have temperatures $T_{\rm eff}\geq$140 000 K, and the X-rays are of thermal origin in the hot photospheres. It could be shown that the non-detection of "cooler" PG 1159 stars is the consequence of a very strong O VI edge near 100Å. The strength of this edge arises from the high oxygen abundance (of the order 10% by mass) in these carbon/helium dominated stars. Further details on these interesting objects may be found in recent reviews by Dreizler et al. (1995) and Werner et al. (1996a).

The first PG 1159 star discovered from its X-ray properties was H 1504+65 (Nousek et al. 1986). The first ROSAT selected PG 1159 star is RX J 2117.1 +3412, which was analyzed with NLTE model atmospheres using PSPC data

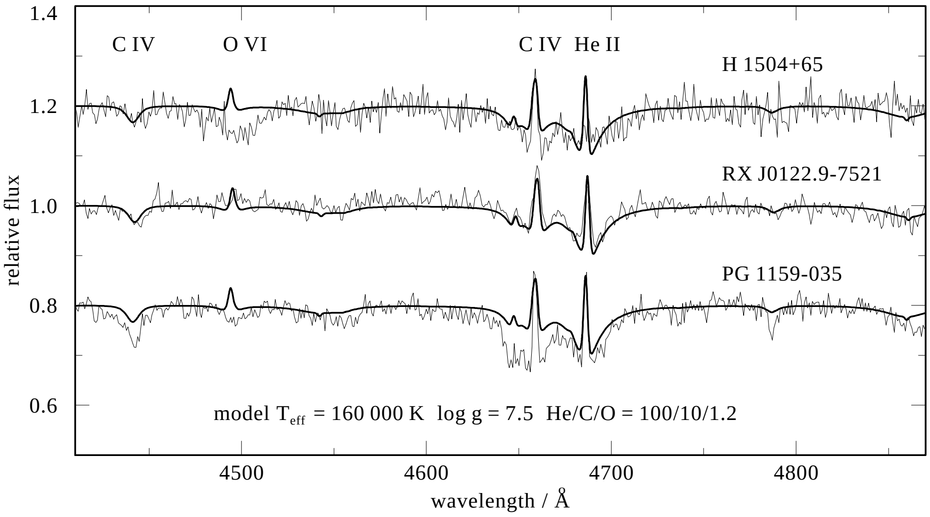

Fig. 1. Optical spectrum of RX J0122.9−7521 (middle) around the characteristic C IV/He II absorption trough region in comparison with spectra from H 1504+65 (top) and the prototype PG 1159−035 (bottom). To facilitate the comparison, overplotted on all three observations is the synthetic spectrum of a model with parameters as given in the panel. The weaker C IV 4660Å and absent O VI 4500Å absorptions in RX J0122.9−7521 are indicative of lower C and O abundances.

as well as optical spectra (Motch et al. 1993). The second ROSAT discovery is RX J0122.9–7521 (Cowley et al. 1995), and we present a similar analysis in this paper. Although RX J0122.9−7521 lies somewhat far from the main body of the Small Magellanic Cloud it was suspected to be a SMC member (Kahabka et al. 1994). Its identification as a PG 1159 star by Cowley et al. 1995 made its SMC membership rather unlikely and we will show that it is in fact a Galactic foreground object. A comparison of visual and X-ray fluxes of both ROSAT discovered stars reveals an unusually high X-ray luminosity for the new PG 1159 star. Although visually fainter by almost 2 magnitudes, the PSPC count rate of RX J0122.9−7521 is more than twice as high as compared to RX J 2117.1+3412 (see Table 1). Our analysis aims at clarifying this behavior.

2 Model Atmospheres and Observations

Synthetic optical and X-ray spectra are computed with a NLTE model atmosphere code developed at Kiel/Bamberg/Potsdam institutes (for numerical details see Dreizler & Werner 1993). The models are plane-parallel and assume hydrostatic and radiative equilibrium. Model atmospheres which are particularly tailored for the analysis of optical and X-ray spectra of PG 1159 stars are described in Werner et al. (1991) and Motch et al. (1993).

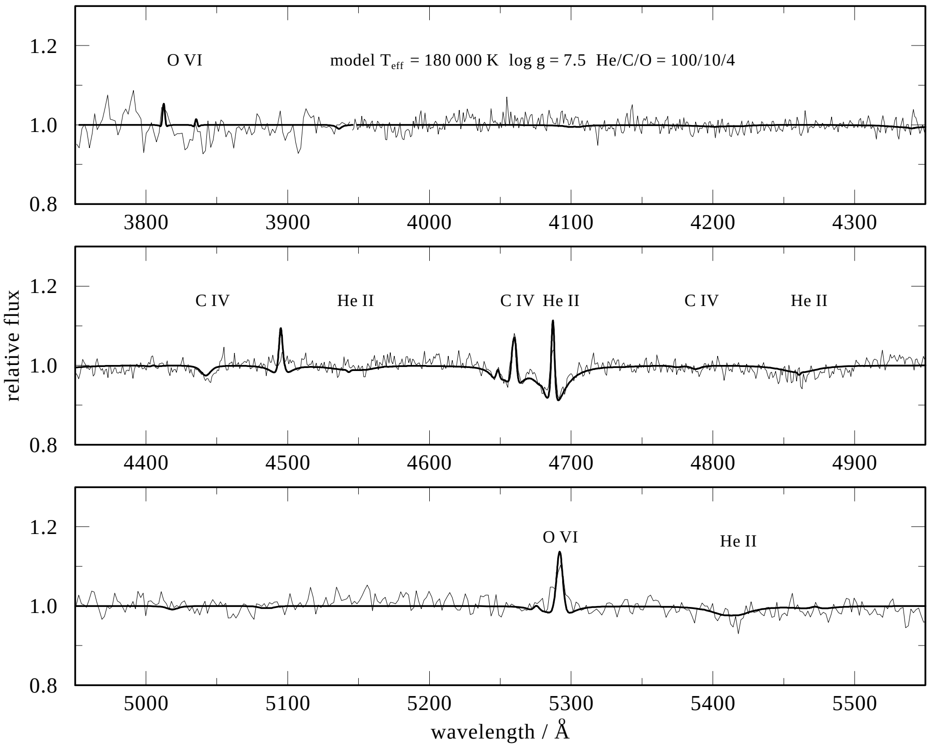

Fig. 2. The complete optical spectrum of RX J0122.9−7521 taken from Cowley et al. (1995). Besides the lines already identified in the close-up in the preceding figure, there is only one additional prominent feature, an emission from O VI 5290Å. Overplotted is the spectrum of the model with the finally adopted parameters.

A hint as to the extraordinarily high X-ray luminosity of RX J0122.9−7521 is immediately evident in Fig. 1 from a comparison of its optical spectrum with those of the prototype star PG 1159−035 and of the above mentioned H 1504+65. It is obvious that the photospheric content of carbon and oxygen in RX J0122.9−7521 is lower than in the comparison stars. Both other stars show a shallow O VI absorption at 4500Å while RX J0122.9−7521 does not, and the depth of the C IV 4660Å absorption complex in RX J0122.9−7521 is much weaker when compared to PG 1159−035. Generally, the appearance of central emission reversals in the C IV 4660Å and He II 4686Å lines indicates that RX J0122.9−7521 is among the hottest members of the PG 1159 group. In fact, a detailed fit to the optical lines (Fig. 2) gives $T_{\rm eff}$=180 000 ± 20 000 K, $\log g$ =7.5±0.5, and an O/He number abundance ratio well below 10% (note that the model predicts an excessively strong O VI 4500Å emission [n=8→10 transitions], which is probably the consequence of a too small model atom). A higher oxygen abundance can be excluded, because otherwise the O VI emission line at 5290Å would be accompanied by shallow absorption wings, as is the case

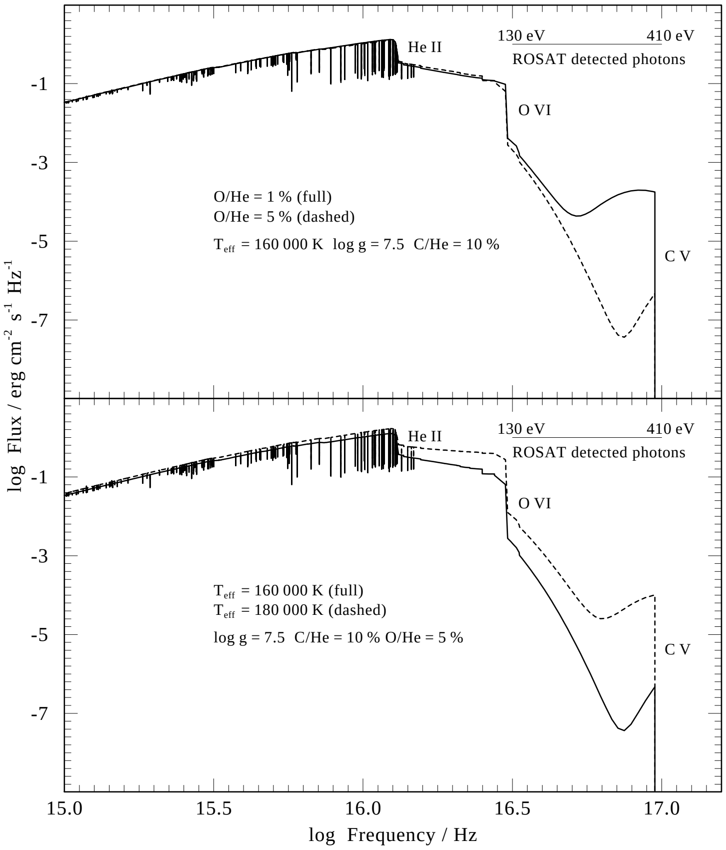

Fig. 3. Top: Flux distribution of two NLTE models with different oxygen abundance. Enhancing the O abundance strengthens the O VI 2p absorption edge at 130 eV and strongly suppresses the secondary flux maximum before the C V ground state edge. The C V edge blocks virtually all photons with energies above 410 eV. Bottom: The influence of the temperature on the soft X-ray flux is extremely strong. Near the C V edge an increase of $T_{\rm eff}$ by 20 000 K produces more than two orders of magnitude more photons.

in the prototype (cf. Werner et al. 1991). The relatively low oxygen abundance is in accordance with the results of our fit to the X-ray spectrum, which will be described below. But in order to understand the basic photospheric features which dominate the X-ray flux let us have a closer look at some models.

In Fig. 3 we compare the fluxes of models which differ in effective temperature and oxygen abundance, demonstrating the effects of these parameters on the emergent spectrum. The figures show the flux distribution from the UV to the soft X-ray region and a horizontal bar indicates the energy range at which photons are detected by the ROSAT PSPC. Two prominent features determine the shape of the soft X-ray flux. The first is a strong O VI edge at 130 eV and

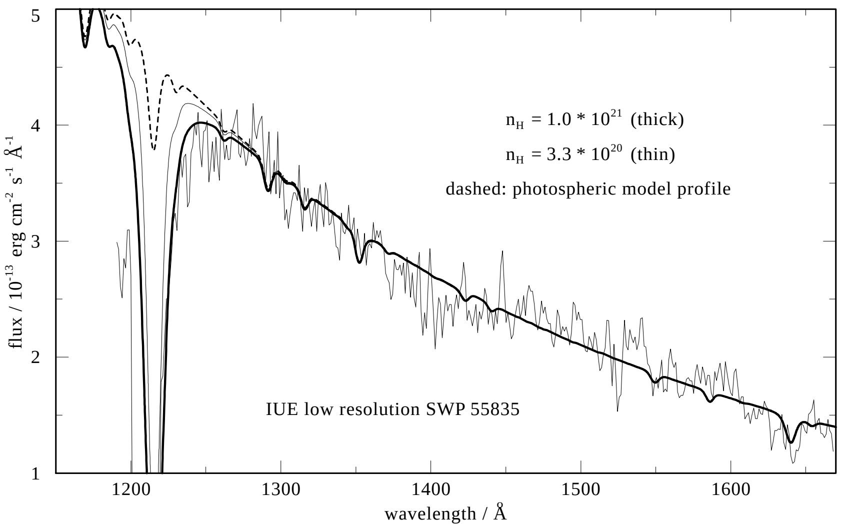

Fig. 4. An attempt to constrain the interstellar hydrogen column density towards RX J0122.9−7521 by a fit to the Ly α red wing fails. See discussion in the text. Due to the high noise, no line features except from interstellar species can be identified.

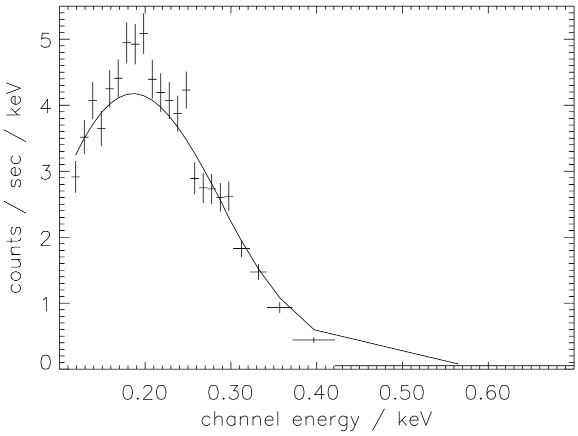

Fig. 5. Best model fit to the observed PSPC pulse height distribution. Model parameters are equal to those for the optical line fit shown in Fig. 2. The resulting interstellar column density amounts to $N_H = 2.6 \cdot 10^{20}$. The pointed observation was performed in Sept./Oct. 1993 and retrieved from the ROSAT archive.

the second is the even stronger C v ground state edge at 410 eV which virtually blocks all the higher energy photons in every model relevant to the present analysis (for a discussion of NLTE models with much higher temperatures, see contributions by Rauch (1996) and Hartmann (1996). Hence, the only feature

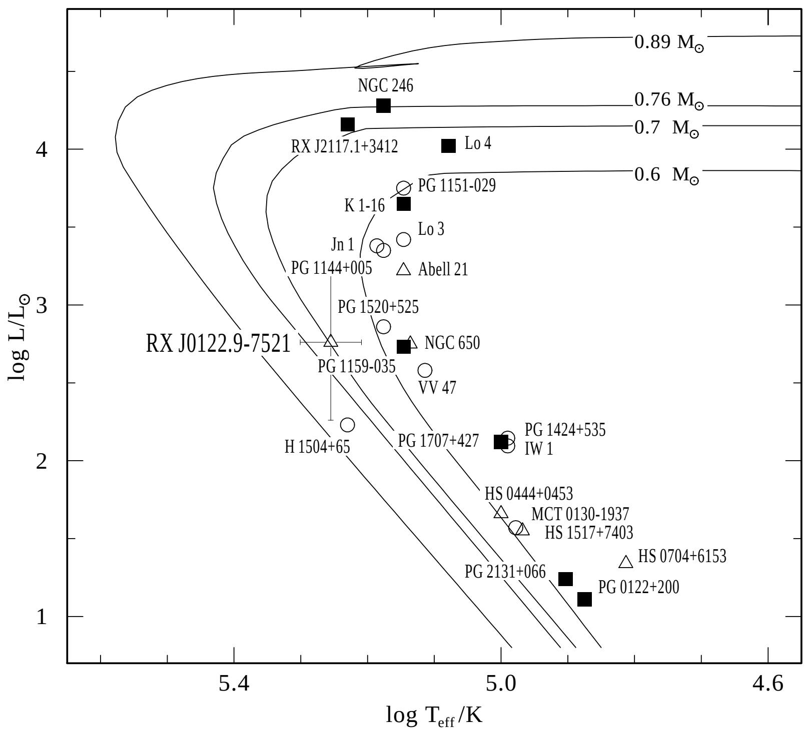

Fig. 6. Position of RX J0122.9−7521 (with error bars) in the HR diagram. It lies on a 0.7 $M_\odot$ post-AGB evolutionary track and represents a descendant of the much more luminous RX J 2117.1+3412. Also shown are positions of previously analyzed PG 1159 stars (different symbols for pulsators □, non-pulsators ○, and unknown photometric behavior △) as taken from Werner et al. (1996a). Evolutionary tracks are from Wood & Faulkner (1986).

which remarkably changes the soft X-ray flux is the O VI edge. From Fig. 3 we learn that $T_{\rm eff}$ as well as the O abundance are the two key parameters which determine the strength of the edge. It follows that the analysis of the X-ray data alone gives no useful results, but that the optical spectra have to be used for a sensible interpretation. It should be noted that a change in the surface gravity, within the limits from the optical analysis, leaves the X-ray flux almost unaffected. The same holds for the C/He abundance ratio which is – like $\log g$ – fixed from the optical line profiles.

Interstellar absorption is another unknown parameter which enters the X-ray analysis so it would be most useful to get an independent estimate of the H column density ($N_{\rm H}$) towards RX J0122.9−7521. We have obtained a IUE low resolution spectrum hoping to constrain $N_{\rm H}$ by fitting the Ly α wing. In Fig. 4 we show the IUE spectrum together with the photospheric model flux and the same flux attenuated by two different values for $N_{\rm H}$ (in $\rm cm^{-2}$). The lower value ($N_H = 3.3 \cdot 10^{20}$) represents the Galactic column density towards the SMC (Bessell 1991) and hence should be an upper limit for RX J0122.9−7521. It seems that this value is too low to fit to the observed profile and that a value three times higher fits better. This is, of course, unreasonably high and analysis of the X-ray spectra (see below) gives a value of $2.6 \cdot 10^{20}$. We can only speculate about reasons for the failure to get an acceptable fit to Ly α, e.g. the IUE spectrum is rather noisy and it is difficult to define the continuum. As a consequence, the interstellar column towards RX J0122.9−7521 must be treated as an unknown parameter. Fig. 5 shows our best fit model to the observed pulse height distribution. The model ($T_{\rm eff}$=180 000 K) was selected from a grid which covers $T_{\rm eff}$=150 000–200 000 K and O/He=0.5–10 (% number ratio). The fit is not perfect but represents a compromise. The model flux is too low by about 20% at the observed peak height (near 0.2 keV), but somewhat too high at the highest observed energies. Increasing $T_{\rm eff}$ improves the low energy fit but at the hard end the flux excess becomes too strong. The opposite holds for decreasing $T_{\rm eff}$. Although the shape of the flux distribution can be fitted with the adopted oxygen abundance, it could be slightly improved with a higher O/He value (along with a slight increase of $T_{\rm eff}$ in order to compensate for the stronger O VI edge). But then the optical O VI 5290Å emission line develops absorption wings which are not observed.

Table 1. Comparison of results from NLTE analyses of RX J 2117.1+3412 (Motch et al. 1993, Werner et al. 1996b) and of RX J0122.9−7521 (this work)

	RX J 2117.1+3412	RX J0122.9−7521
V-magnitude	13.2	15.4
PSPC ct/s	0.33	0.81
$T_{\rm eff}$/1000 K	170	180
$\log g$ (cgs)	6.0	7.5
He/C/O mass fractions (%)	33/50/17	68/21/11
N_H/cm^{-2}	$3.2 \cdot 10^{20}$	$2.6 \cdot 10^{20}$
$\log(L/L_\odot)$	4.16	2.76
$\log(R/R_\odot)$	-0.89	-1.6
$M/M_\odot$	0.70	0.70
distance/pc	1400	700

3 Summary

RX J0122.9−7521 is the hottest known PG 1159 star (see Fig. 6), closely followed by RX J 2117.1+3412 (see Motch et al. 1993 and a refined analysis with HST spectra by Werner et al. 1996b). Table 1 summarizes the results of the present analysis and compares the properties of both ROSAT discovered objects. The higher X-ray luminosity of RX J0122.9−7521 is a consequence of both its slightly higher effective temperature and its relatively low oxygen abundance. In addition, the interstellar hydrogen column density is lower, but there remains a discrepancy with the IUE Ly α profile. Comparing the position of both stars in the $T_{\rm eff}$–$\log g$ diagram reveals very similar masses. However, the deduced total luminosity of RX J0122.9−7521 shows that it is more evolved than RX J 2117.1+3412 (roughly 10^4 years higher post-AGB age). Comparing the measured V magnitude with the model flux clearly rules out SMC membership of RX J0122.9−7521. It yields a distance determination of 700^{+550}_{-310} pc.

We remark that RX J0122.9−7521 has no associated planetary nebula while about 50% of the PG 1159 members are central stars. In addition, it is located outside of the GW Vir instability strip (Werner et al. 1996c), hence we do not expect that RX J0122.9−7521 exhibits photometric variability. In fact, no obvious variability was detected by Cowley et al. (1995) and Bond (1996). Other questions not addressed here concern the possible detection of line profile variations as well as weak N V emission lines in some spectra. These findings deserve further attention.

Acknowledgement: ROSAT data analysis at Kiel and Potsdam is supported by the DARA under grant 50 OR 9409 1. Stefan Jordan kindly supplied his INTEX tool for ROSAT data analysis.

References

Bessell M.S., 1991, A&A 242, L17
Bond H.E., 1996, private communication
Cowley A.P., Schmidtke P.C., Hutchings J.B., Crampton D., 1995, PASP 107, 927
Dreizler S., Werner K., 1993, A&A 278, 199
Dreizler S., Werner K., Heber U., 1995, in White Dwarfs, eds. D. Koester and K. Werner, Lecture Notes in Physics 443, Springer, Berlin, p. 160
Hartmann H.W., Heise J., 1996, this volume p. 6
Kahabka P., Pietsch W., Hasinger G., 1994, A&A 288, 538
Motch C., Werner K., Pakull M.W., 1993, A&A 268, 561
Nousek J.A., Shipman H.L., Holberg J.B., et al. , 1986, ApJ 309, 230
Rauch T., 1996, this volume p. 3
Werner K., 1996, in Röntgenstrahlung from the Universe, eds. H.U. Zimmermann, J.E. Trümper, H. Yorke, MPE Report 263, p. 205
Werner K., Heber U., Hunger K., 1991, A&A 244, 437
Werner K., Dreizler S., Heber U., Rauch T., 1996a, in Hydrogen-Deficient Stars, eds. U. Heber and C.S. Jeffery, The ASP Conference Series, p. 267
Werner K., Dreizler S., Heber U., Rauch T., Fleming T.A., Sion E.M., Vauclair G., 1996b, A&A 307, 860
Werner K., Dreizler S., Heber U., Rauch T., 1996c, in Astrophysics in the Extreme Ultraviolet, IAU Colloquium 152, eds. S. Bowyer and R.F. Malina, Kluwer, p. 229
Wood P.R., Faulkner D.J., 1986, ApJ 307, 659

Implications of Light Metals (Li - Ca) on NLTE Model Atmospheres for Hot Stars

T. Rauch

Universität Kiel, Institut für Astronomie und Astrophysik, Germany
Universität Potsdam, Lehrstuhl Astrophysik, Germany

Abstract. Neither iron line-blanketed LTE model atmospheres nor "standard" NLTE models (including H, He, C, N, O, Ne) can reproduce the observed stellar EUV and X-ray fluxes of hot stars: huge differences appear at energies higher than 54 eV (He II Lyman continuum) which are a result of light metal opacities which have a strong influence on the emergent fluxes of hot stars in this energy range. These metal opacities have not been included in "standard" NLTE model atmosphere calculations so far. We present NLTE model atmospheres including all elements from hydrogen to calcium.
In order to calculate more realistic stellar fluxes, such models should preferentially be used for the EUV and X-ray analysis of very hot stars instead of black bodies which are often used in the analysis of X-ray spectra.

1 Introduction

In the last quarter of this century the numerical models for the interpretation of spectra of hot stars have been continuously improved.

In 1969 Auer & Mihalas presented the complete linearization method for the calculation of "Classical Models". These were limited due to numerical reasons and missing computational capacities — only a handful of NLTE levels and line transitions could be considered.

The rapidly evolving observational techniques provided UV and X-ray spectra (e.g. IUE, Einstein, and EXOSAT satellites) and high-resolution optical spectra (e.g. ESO CASPEC) and have been a challenge for theory: In 1985 Werner & Husfeld presented the newly developed accelerated lambda iteration (ALI) technique for line formation calculations. This method was later applied to the calculation of NLTE model atmospheres (Werner 1986). Presently calculated model atmospheres treat over 200 atomic levels in NLTE and consider more than 10^6 line transitions.

Further progress in observation (e.g. HST, ROSAT, EUVE, ISO, and the ESO VLT) requires adequate models, tailored for an interpretation of the complete wavelength range from the far infrared to the X-ray region.

For "cool" stars ($T_{\rm eff}< 30$ kK, spectral type B or later), the fully line blanketed LTE models (Kurucz 1979, 1991) are available, which consider all elements up to the iron group and the blanketing of millions of lines.

The present state-of-the-art NLTE models (Dreizler & Werner 1993, Rauch 1996b) include also all elements up to the iron group (including line blanketing) and permit to perform analyses of very hot stars with realistic models.

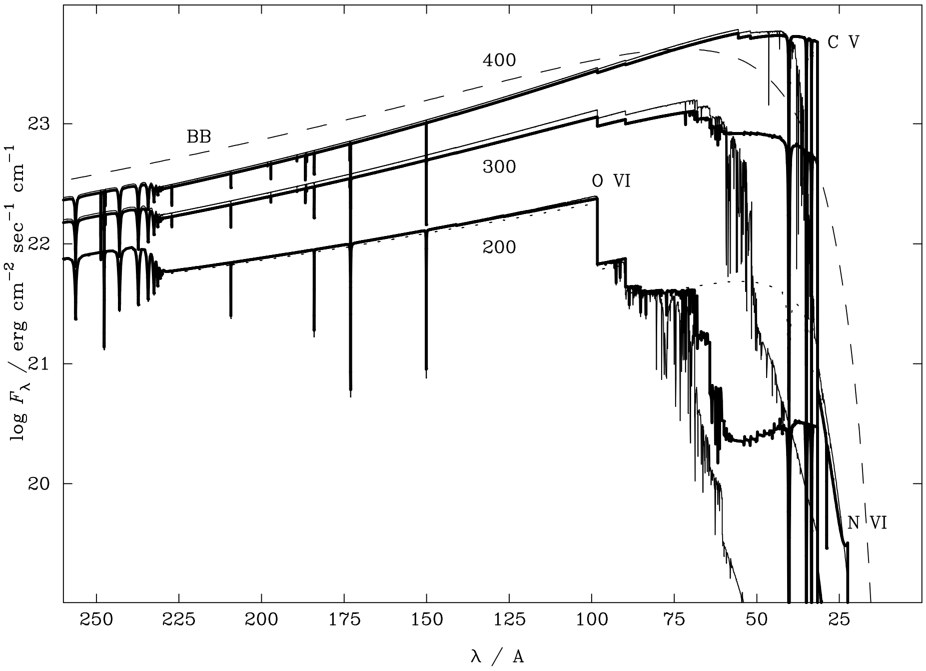

Fig. 1. Emergent fluxes of NLTE model atmospheres with $\log g = 8$, $T_{\rm eff} = 200$, 300, 400 kK, and solar abundances calculated with H+He+C+N+O (200 kK only, dotted line) and H+He+C+N+O+Ne (▬) compared to those of H - Ca (—) models. The dashed line is the flux of a black body (BB) with 400 kK. Note the strong absorption edges of O VI 2p at 98 Å and 2s at 89 Å which almost disappear at $T_{\rm eff} = 400$kK due to the changing ionization equilibrium, and the much stronger ground state absorption edge of C V at 31.6 Å which will also disappear towards higher $T_{\rm eff}$ (Fig.2).

2 NLTE Model Atmospheres

Our model atmospheres are plane parallel, chemically homogeneous, and in radiative and hydrostatic equilibrium. They were calculated using the ALI method.

While the implications of H, He, C, N, and O (Rauch 1993) and of the iron group elements on NLTE model atmospheres have been studied in detail (Dreizler & Werner 1993), the light metals lithium through calcium have been regarded as trace elements and were neglected in model atmosphere calculations so far. For some of them line formation calculations (i.e. fixed atmospheric structure) had been carried out in order to determine photospheric abundances, e.g. Dreizler (1993) for Ne, Mg, Si in sdO stars. However, the "total abundance" of the light metals is comparable to that of the CNO elements and thus, not negligible.

In the construction of our model atoms we have to consider that the number of tractable NLTE levels is restricted due to numerical accuracy (< 200). Thus,

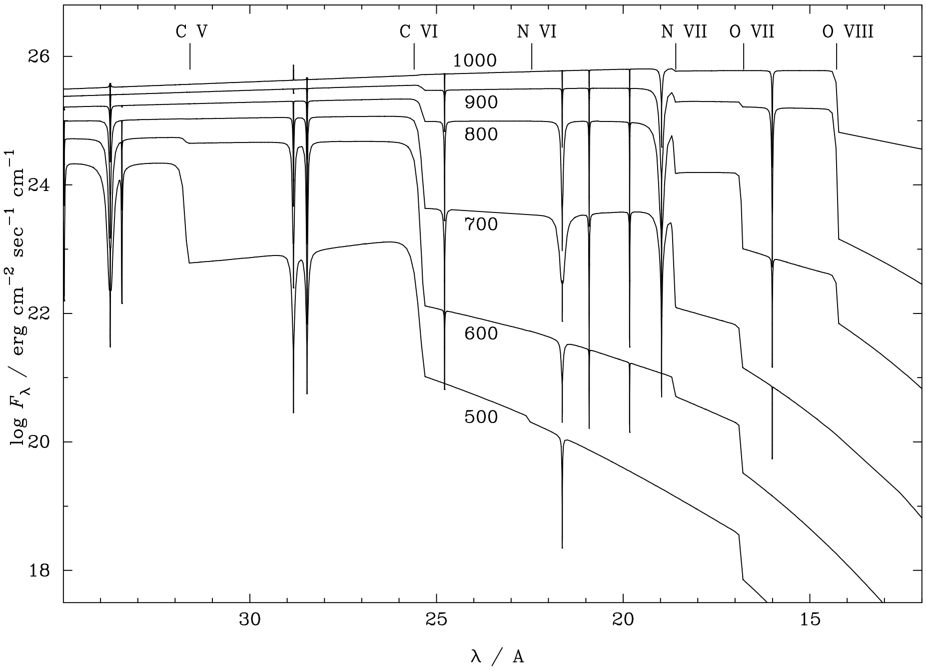

Fig. 2. Emergent fluxes of H+He+C+N+O NLTE model atmospheres (including lines) with $\log g = 9$, $T_{\rm eff} = 500, \ldots, 1000$ kK, and solar abundances. The wavelengths of the ground state thresholds of C V, C VI, N VI, N VII, O VII, and O VIII are marked. Note that their edges appear always in absorption, and have a maximum at that $T_{\rm eff}$, where the respective ion dominates in the atmosphere due to the ionization equilibrium (e.g. N VII at $\approx$ 700 kK, O VIII at $\approx$ 900 kK).

we used "standard" model atoms for H and He (e.g. Rauch 1993) and small model atoms for C, N, and O. In test calculations, Li, Be, and B were found to be unimportant and neglected. F - Ca were represented by model atoms "as small as possible, as large as necessary" in order to consider all ionization stages that dominate in certain parts of the atmosphere as well as resonance lines. Their photoionization cross-sections were calculated using Opacity Project (cf. Seaton et al. 1994) data.

The changes in the temperature stratification due to the consideration of metals, especially of their resonance lines are demonstrated by Rauch (1996a). The differences in the atmospheric structure have a direct influence on theoretical profiles of e.g. H I and He II lines, which are used in spectral analyses to determine $T_{\rm eff}$, $\log g$, and the photospheric He/H abundance ratio. This is shown in detail by Rauch (1996b).

3 Emergent Flux

In Fig. 1 we show the emergent fluxes of models which are calculated with different $T_{\rm eff}$ and chemical compositions. Obviously, metal opacities reduce the flux in the EUV and X-ray range by orders of magnitude. A comparison to the flux of a black body (BB, at 400 kK, Fig. 1) shows that a BB is unsuitable for analyses of most stars: The BB flux maximum is at ≈ 72 Å while the NLTE flux maximum is at ≈ 50 Å — and at a higher ($\approx 20\%$) flux level. A similar result was found by Heise et al. (1994): Their LTE model atmospheres are also more efficient soft X-ray emitters than BBs but the resulting LTE spectra are much flatter (at a lower flux level than the BBs!).

4 Summary

Emergent fluxes calculated from NLTE model atmospheres which include the "light metals" F - Ca show a drastic decrease of the flux level at energies higher than 126 eV (= O VI 2p continuum) compared to that of "standard" (H+He+C+N+O+Ne) models.

However, at a given $T_{\rm eff}$, NLTE and LTE model atmospheres have their flux maxima at higher energies than a BB. The flux level of a NLTE model is higher than that of a LTE model (this will be investigated in a forthcoming paper).

For a realistic X-ray analysis of very hot stars the use of NLTE model atmospheres which consider metal opacities is highly recommended.

Acknowledgement: This research was supported by the DARA under grant 50 OR 9409 1.

References

Auer L.H., Mihalas D., 1969, ApJ 158, 641
Dreizler S., 1993, A&A 273, 212
Dreizler S., Werner K., 1993, A&A 278, 199
Heise J., Van Teeseling A., Kahabka P., 1994, A&A 288, L45
Kurucz R.L., 1979, ApJS 40, 1
Kurucz R.L., 1991, in: Stellar Atmospheres: Beyond Classical Models, eds. L. Crivellari, I. Hubeny, D.G. Hummer, NATO ASI Series C, Vol. 341, p. 44
Rauch T., 1993, A&A 276, 171
Rauch T., 1996a, in: Röntgenstrahlung from the Universe, eds. H.U. Zimmermann, J.E. Trümper, H. Yorke, MPE Report 263, p. 63
Rauch T., 1996b (in prep.)
Seaton M.J., Yu Yan, Mihalas D., Pradhan A.K., 1994, MNRAS 266, 805
Werner K., 1986, A&A 161, 177
Werner K., Husfeld D., 1985, A&A 148, 417